J. Fluid Mech. (2010), *vol.* 663, *pp.* 180–208. © Cambridge University Press 2010
doi:10.1017/S0022112010003435

Slug genesis in cylindrical pipe flow

Y. DUGUET,[1,2,4]† A. P. WILLIS [1,3] AND R. R. KERSWELL[1]

[1]School of Mathematics, University of Bristol, BS8 1TW Bristol, UK

[2]Linné Flow Centre, KTH Mechanics, SE-100 44 Stockholm, Sweden

[3]Laboratoire d'Hydrodynamique, Ecole Polytechnique, 91128 Palaiseau, France

[4]LIMSI-CNRS, UPR 3251, 91403 Orsay, France

(Received 19 January 2010; revised 24 June 2010; accepted 24 June 2010;
first published online 5 October 2010)

Transition to uniform turbulence in cylindrical pipe flow occurs experimentally via the spatial expansion of isolated coherent structures called 'slugs', triggered by localized finite-amplitude disturbances. We study this process numerically by examining the preferred route in phase space through which a critical disturbance initiates a 'slug'. This entails first identifying the relative attractor – 'edge state' – on the laminar–turbulent boundary in a long pipe and then studying the dynamics along its low-dimensional unstable manifold, leading to the turbulent state. Even though the fully turbulent state delocalizes at $Re \approx 2300$, the edge state is found to be localized over the range $Re = 2000$–6000, and progressively reduces in both energy and spatial extent as Re is increased. A key process in the genesis of a slug is found to be vortex shedding via a Kelvin–Helmholtz mechanism from wall-attached shear layers quickly formed at the edge state's upstream boundary. Whether these shedded vortices travel on average faster or slower downstream than the developing turbulence determines whether a puff or a slug (respectively) is formed. This observation suggests that slugs are out-of-equilibrium puffs which therefore do not co-exist with stable puffs.

Key words: pipe-flow boundary layer, transition to turbulence, turbulence simulation

1. Introduction

The laminar flow of a Newtonian fluid inside a straight pipe of circular cross-section is known to undergo a transition to turbulence as the flow rate is increased, producing a dramatic rise in skin friction. Reynolds (1883) was the first to identify the 'Reynolds' number $Re := UD/\nu$ as the sole controlling parameter for the flow, where U is the bulk velocity, D the diameter and ν the kinematic viscosity. Reynolds reported that the transition typically occurs for $Re \approx 2000$, a commonly quoted value in textbooks and widely reproduced ever since (critical Re reported vary across the range 1760–2300, e.g. Binnie & Fowler 1947, Lindgren 1958, Leite 1959, Wygnanski & Champagne 1973 and Darbyshire & Mullin 1995). Reynolds was also aware that if extra care was taken to reduce the amplitude of disturbances at the inlet, transition could be delayed (reportedly to $\approx 12\,000$), emphasizing the dependence of transition on the ambient noise level present and hence the inherently finite-amplitude nature of the process. By way of confirmation, Pfenniger (1961) managed to keep the flow laminar in a very well controlled experiment until $Re \approx 10^5$.

† Email address for correspondence: duguet@mech.kth.se

https://doi.org/10.1017/S0022112010003435 Published online by Cambridge University Press

When transition is triggered, turbulence first appears at isolated locations (not necessarily at the inlet), before expanding ($Re \gtrsim 2300$) to contaminate the whole downstream domain (Reynolds 1883; Lindgren 1958, 1969; Wygnanski & Champagne 1973; Mullin 2010). These growing patches of turbulent motion, which fill the whole cross-section of the pipe and are separated from each other by laminar regions, were called 'flashes' by Reynolds. Later a distinction was drawn between two different states christened 'puffs' and 'slugs' (Wygnanski & Champagne 1973). Turbulent puffs correspond to a turbulent region with a sharp upstream boundary – the trailing edge (TE) – but whose downstream border – the leading edge (LE) – is much less well-defined, containing more large-scale structures which appear to decay away. They are observed experimentally for $Re \lesssim 2700$ (Wygnanski & Champagne 1973) provided a large enough disturbance is applied to the flow, and for $Re \approx 1750$–2200, they tend to keep a constant length of about 20 pipe diameters as they propagate downstream. For $Re \gtrsim 2700$, slugs can be clearly identified in which the downstream boundary is reported to be as sharp as the upstream one. The enclosed turbulent motion, which fills the whole cross-section of the pipe, then looks indistinguishable from a fully turbulent pipe flow (Wygnanski & Champagne 1973). The upstream front moves slower than the mean flow speed whereas the downstream moves faster, so that the slug grows in length as it is advected down the pipe (Lindgren 1969; Wygnanski & Champagne 1973; Nishi *et al.* 2008). Little is known so far about the intermittent regime, intermediate between the puff and the slug regime. It is characterized by the disordered co-existence of laminar and turbulent domains in which puffs split and merge and possess sharpened slug-like LEs (Moxey & Barkley 2010).

Given this background, two key questions are the following. What are the mechanisms by which puffs and slugs are formed? And what are the important processes which allow a puff to adopt an 'equilibrium' length but forces a slug to expand aggressively? Efforts to explain the observed behaviour initially concentrated on establishing the linear stability of the laminar Hagen–Poiseuille flow (Hagen 1839 & Poiseuille 1840). Stability was proved under the assumption of axisymmetry (Herron 1991), and demonstrated in the general case up to $Re = 10^7$ (Meseguer & Trefethen 2003). At the other end of the spectrum, Joseph & Carmi (1969) also proved that any disturbance would decay monotonically provided $Re < 81.49$. The next logical step was to search for the emergence of alternative solutions between these two extremes, in the hope that this would make sense of the $O(2000)$ transition point. Despite some early success by Nagata (1990), who identified a steady-state solution in plane Couette flow, it was not until Waleffe (1997, 1998) uncovered the 'self-sustaining cycle' that it became clear how to find these new states. In a pipe flow, they take the form of travelling waves (TWs) (Faisst & Eckhardt 2003; Wedin & Kerswell 2004; Pringle & Kerswell 2007; Pringle, Duguet & Kerswell 2009). Experimental observations (Hof *et al.* 2004) and numerical experiments in short periodic pipes (Kerswell & Tutty 2007; Schneider, Eckhardt & Vollmer 2007*a*) demonstrated that these solutions appear fleetingly as coherent structures in pipe turbulence.

Work directed at establishing the role of these states in transition has tended to focus on the theoretical model of a short (typically $5D$ long) pipe along which periodic boundary conditions are imposed. Not only does this eliminate the issue of co-existence of turbulent- and laminar-flow regions, but it is much more efficient to simulate numerically. Following the work of Itano & Toh (2001) in a plane Poiseuille flow, a key advance by Schneider, Eckhardt & Yorke (2007*b*) was to realize that the laminar–turbulent boundary Σ – the separatrix between the two local attractors – could be traced numerically. By studying the dynamics restricted to this boundary,

https://doi.org/10.1017/S0022112010003435 Published online by Cambridge University Press

it became clear that 'lower branch' TWs are embedded within it (Duguet, Willis & Kerswell 2008), so that initial conditions arbitrarily close to one of these TWs could either lead to turbulence or relaminarize (see e.g. Kerswell & Tutty 2007, as well as Viswanath 2007 and Wang, Gibson & Waleffe 2007 for plane Couette flow). Considerable progress has been made by viewing this restricted form of pipe flow and other shear flows as a huge dynamical system (see the review by Eckhardt *et al.* 2007 for a pipe flow, Viswanath 2007, Gibson, Halcrow & Cvitanovic 2008, 2009 and Halcrow *et al.* 2009 for plane Couette flow).

The spatiotemporal dynamics of real pipe flows is, however, less clearly amenable to dynamical systems thinking as the flow is no longer in either the laminar or the turbulent state globally. As a result, our understanding is much more modest; yet only here is true contact possible with experimental observations. Fortunately, direct numerical simulation is now feasible in sufficiently long computational pipes ($\gtrsim 30\,D$ long) to realistically capture 'puff' and 'slug' structures in pipe flow (Leonard & Reynolds 1985; Shan *et al.* 1999; Priymak & Miyazaki 2004; Reuter & Rempfer 2004; Willis & Kerswell 2007, 2008; Shimizu & Kida 2008, 2009; Mellibovsky *et al.* 2009; Willis *et al.* 2009; Moxey & Barkley 2010).

Very recent investigations (Shimizu & Kida 2009; Hof *et al.* 2010) have proposed a mechanism for the sustenance of a turbulent puff, thereby opening the way for active control strategies. The suggested mechanism focuses on the role of local instabilities occurring upstream of the turbulent flow, triggering turbulent fluctuations which are convected downstream into the puff to presumably re-energize the vorticity field in the puff against slow viscous decay. These fluctuations initially take the form of rolled-up vortices emanating from the shear layer upstream of the puff (Bandhyopadyay 1986). Numerical simulation at higher Re appears to be an adequate tool to investigate what becomes of this suggested mechanism in a non-equilibrium situation such as that of an expanding slug. The purpose of this paper is therefore to investigate how a slug is formed and to examine the relevance of this mechanism in the process. The key to this is identifying a natural starting point for detailed simulations. The edge state provides just such an initial condition because (*a*) its unstable manifold directed across the laminar–turbulent boundary must lead to a slug being formed and (*b*) arbitrary initial conditions close to and 'above' the threshold for triggering a slug will first shadow the laminar–turbulent boundary, being attracted towards the edge state, before being flung off along its unstable manifold (see the sketch in figure 1). Choosing to initiate our simulations in the neighbourhood of the edge state thus ensures that the evolution of the flow is least affected by the shape of an artificially prescribed initial condition. Following a flow trajectory starting very near the edge state also corresponds in phase space to the experimental situation when the amplitude of a disturbance is increased just enough to trigger turbulence. Therefore, our first (preliminary) objective is to compute the edge state at sufficiently high Re ($\gtrsim 2700$), which is appropriate for slugs to exist. Then the second (main) objective is to study how the flow metamorphoses into an expanding slug along the unstable manifold of the edge state.

This paper is organized as follows. In §2 we present the numerical tools used throughout the paper. Section 3 details the computation of edge states up to $Re = 6000$, extending previous recent computations (Mellibovsky *et al.* 2009; Willis & Kerswell 2009) which reported that the edge state stays localized even when the turbulent state is not. An interesting new observation made here is that the edge state becomes progressively smoother in both a spatial (as noted in Mellibovsky *et al.* 2009) and a temporal sense with increasing Re, culminating, if the dynamics are suitably restricted as well, in what appears to be a simple spatially localized TW. Section 4 then

https://doi.org/10.1017/S0022112010003435 Published online by Cambridge University Press

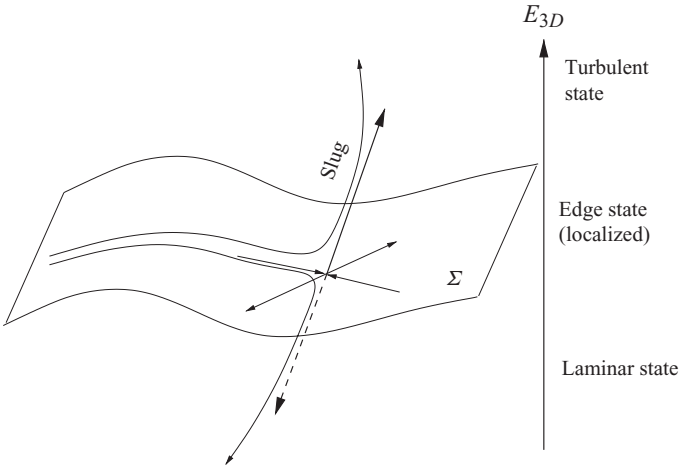


FIGURE 1. Schematic view of the neighbourhood of an unstable exact state (e.g. TW) on the laminar–turbulent boundary Σ. For $Re > 2700$, the part of the unstable manifold which is not tangent to Σ and points towards the turbulent state is expected to correspond to a slug in physical space. The symbolic axis E_{3D} refers to the energy contained in the strictly three-dimensional part of the flow.

studies the generation of a slug when the edge state is perturbed. Particular attention is paid to the shear instability occurring along the edge → turbulence route, and to the role of the subsequent vortical fluctuations appearing at the TE in determining whether an equilibrium puff, intermittency or a slug is set up. A discussion follows in § 5.

2. Numerical procedure

We consider the incompressible flow of a Newtonian fluid in a straight pipe of cylindrical cross-section and adopt the usual set of cylindrical coordinates (s, θ, z) aligned with the pipe axis and velocity components, $\boldsymbol{u} = u\hat{\boldsymbol{s}} + v\hat{\boldsymbol{\theta}} + w\hat{\boldsymbol{z}}$. The domain considered here is $(s, \theta, z) \in [0 : 1/2] \times [0 : 2\pi] \times [0 : L]$, where lengths are in units of diameter D and the pipe length is L diameters. The fluid density is chosen to be unity. The flow is described by the incompressible three-dimensional Navier–Stokes equations:

$$\frac{\partial \boldsymbol{u}}{\partial t} + (\boldsymbol{u}\cdot\nabla)\,\boldsymbol{u} = -\nabla p + \frac{1}{Re}\nabla^2\boldsymbol{u}, \tag{2.1}$$

$$\nabla\cdot\boldsymbol{u} = 0. \tag{2.2}$$

where, recall, $Re := UD/\nu$, with ν being the kinematic viscosity and U the bulk axial velocity. U is held fixed to maintain constant mass flux as in recent experiments (e.g. Peixinho & Mullin 2006). Energies integrated over the pipe volume are expressed in units of U^2D^3 and time in units of D/U. The boundary conditions are periodicity along the pipe length $\boldsymbol{u}(s, \theta, z) = \boldsymbol{u}(s, \theta, z+L)$ and no-slip on the walls $\boldsymbol{u}(1/2, \theta, z) = \boldsymbol{0}$.

2.1. *Definitions*

We use the mixed finite-difference/spectral code described in Willis & Kerswell (2009) for time-stepping of the incompressible Navier–Stokes equations. Defined on a non-equispaced grid, variables are expanded in the form

$$\Phi(s_j, \theta, z, t; \alpha, m_0) = \sum_{k=-K}^{K}\sum_{m=-M}^{M} \Phi_{jkm}(t)\exp(\mathrm{i}(m_0 m\theta + \alpha k z)). \tag{2.3}$$

https://doi.org/10.1017/S0022112010003435 Published online by Cambridge University Press

The resolution of a given calculation is described by the triplet (N, M, K), and the set of all complex coefficients defines a phase space of dimension $O(8MNK)$, which is typically around 2 million. The positive integer m_0 refers to the discrete rotational symmetry

$$\boldsymbol{R}_{m_0} : (u, v, w, p)(s, \theta, z) \to (u, v, w, p)\left(s, \theta + \frac{2\pi}{m_0}, z\right), \tag{2.4}$$

which can optionally be imposed ($m_0 > 1$) or not ($m_0 = 1$). The positive real number α is defined by $\alpha = \pi/L$. The coefficients $\Phi_{jk\pm m}$, for instance, can also be linked to impose the mirror symmetry

$$\boldsymbol{Z} : (u, v, w, p)(s, \theta, z) \to (u, -v, w, p)(s, -\theta, z). \tag{2.5}$$

Using the notation $\langle \cdot \rangle_A$ to denote averaging over the subscripted variable A, we define the following energies to describe the perturbations (u, v, w) to the parabolic laminar flow:

$$E_{roll}(z, t) := \frac{1}{2} \int_0^{1/2} \int_0^{2\pi} \left((u - \langle u \rangle_\theta)^2 + (v - \langle v \rangle_\theta)^2 \right) \mathrm{d}\theta \, s \, \mathrm{d}s, \tag{2.6}$$

$$E_{streak}(z, t) := \frac{1}{2} \int_0^{1/2} \int_0^{2\pi} (w - \langle w \rangle_\theta)^2 \, \mathrm{d}\theta \, s \, \mathrm{d}s, \tag{2.7}$$

$$E(t) := \frac{1}{2} \int_0^{L} \int_0^{1/2} \int_0^{2\pi} (u^2 + v^2 + w^2) \, \mathrm{d}\theta \, s \, \mathrm{d}s \, \mathrm{d}z, \tag{2.8}$$

$$E_{2d}(t) := \frac{1}{2} \int_0^{1/2} \int_0^{2\pi} \left(\langle u \rangle_z^2 + \langle v \rangle_z^2 + \langle w \rangle_z^2 \right) \mathrm{d}\theta s \, \mathrm{d}s, \tag{2.9}$$

$$E_{3d}(t) := \frac{1}{2} \int_0^{L} \int_0^{1/2} \int_0^{2\pi} \left((u - \langle u \rangle_z)^2 + (v - \langle v \rangle_z)^2 + (w - \langle w \rangle_z)^2 \right) \mathrm{d}\theta \, s \, \mathrm{d}s \, \mathrm{d}z. \tag{2.10}$$

$E_{roll}(z, t)$ represents the kinetic energy associated with the non-axisymmetric cross-stream flow and $E_{streak}(z, t)$ is the kinetic energy associated with the non-axisymmetric axial component of the flow at a given cross-section of the pipe. E is the total kinetic energy associated with the perturbation, E_{2d} is the two-dimensional counterpart associated with the streamwise-averaged flow and E_{3d} is the part of E associated with streamwise-dependent modes.

2.2. *Tracking the laminar–turbulent boundary: bisection*

In order to constrain a phase-space trajectory to stay on the laminar–turbulent boundary Σ, we use the shooting method introduced by Toh & Itano (1999) and more recently refined by Schneider *et al.* (2007*b*). A long turbulent trajectory is simulated and a snapshot $\boldsymbol{u}^*$ of relatively low three-dimensional disturbance energy $E_{3d}(t)$ is selected. An initial condition is then constructed using this field,

$$\boldsymbol{u}_\beta := \langle \boldsymbol{u}^* \rangle_\theta + \beta(\boldsymbol{u}^* - \langle \boldsymbol{u}^* \rangle_\theta), \tag{2.11}$$

parametrized by a real positive number β. (The method also works with axial averaging.) The initial condition $\boldsymbol{u}_{\beta=0}$ is axisymmetric and hence cannot trigger turbulence, whereas $\boldsymbol{u}_{\beta=1}$ is the original turbulent state (or more generally an initial state which leads to turbulence). This interval, $\beta \in [0, 1]$, is bisected until its width is close to that of machine precision, such that, at the upper limit, the initial condition develops into turbulence, and, at the lower limit, it relaminarizes. This forces the

https://doi.org/10.1017/S0022112010003435 Published online by Cambridge University Press

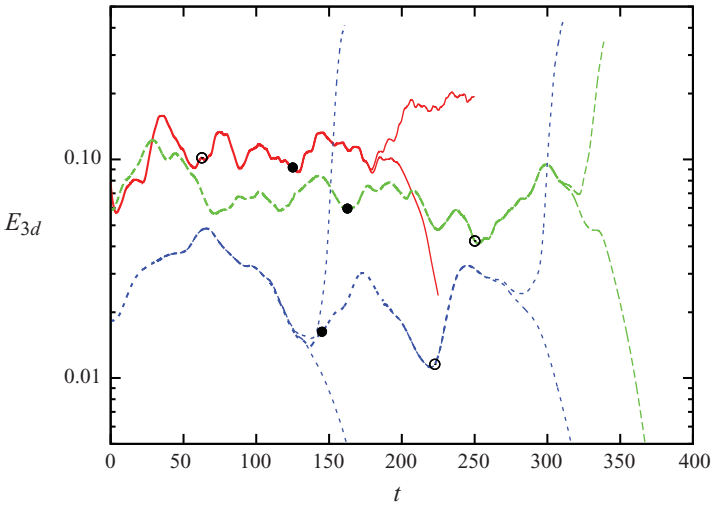


FIGURE 2. (Colour online) $E_{3d}(t)$ of the edge trajectories for $Re = 2000$ (red solid lines), 3000 (green long-dashed lines) and 6000 (blue dashed lines). The filled circles indicate the edge states shown in figure 3 (time is in units of D/U). Filled (respectively open) circles also correspond to the cross-sections in figure 6(a, c, e) left (respectively b, d, f).

trajectory to stay close to the laminar–turbulent boundary for typical times of $O(300\,D/U)$. For the values of Re used here, the values of $E_{3d}(t)$ on Σ are one or several orders of magnitude below those of the turbulence state, thus making the determination of β unambiguous. After bisection, this process can be restarted from nearby states saved near the end of the edge trajectory.

3. Flow on the laminar–turbulent boundary

3.1. *Edge states for* $Re = 2000$, 3000 *and* 6000

Calculations are now presented for edge trajectories in a periodic domain of length $L = 33.51D$ corresponding to $\alpha = \pi/L = 3/32$ at $Re = 2000$, 3000 and 6000. A numerical resolution of $(N, M, K) = (40, 24, 256)$ for $Re \lesssim 4500$ and $(60, 48, 384)$ for $4500 \lesssim Re \leqslant 6000$ proves sufficient to ensure that the power spectrum drops by at least seven decades from lowest to highest order modes for both the edge regime and the turbulent regime. The computational domain is also long enough to simulate localized turbulence (puffs) at $Re = 2000$ and expanding slugs for $Re \geqslant 3000$. Figure 2 shows typical time traces of $E_{3d}(t)$ during the application of the bisection algorithm, for initial conditions consisting of various turbulent puff snapshots calculated at $Re = 2000$. Two features are immediately clear as Re increases: the traces display smoother (lower-frequency) oscillations with more prominent dips, and the mean value of E_{3d} decreases. These observations are consistent with previous work in short pipes (see figure 5 of Schneider & Eckhardt 2009 and figure 7 of Willis & Kerswell 2009), where it is also clear that the edge energetically approaches the laminar state and diverges away from the turbulent state when Re increases (see figures 5 and 7 of Schneider & Eckhardt 2009). The situation is not so simple in a longer domain, as figure 3 indicates. Here snapshots of the axial vorticity are plotted after the edge has been tracked for $O(150\,D/U)$, showing that the flow stays localized in the axial direction for all three Re. Localization is to be expected for $Re = 2000$, where the turbulent state is also localized, but is relatively surprising for $Re \gtrsim 2300$, where

https://doi.org/10.1017/S0022112010003435 Published online by Cambridge University Press

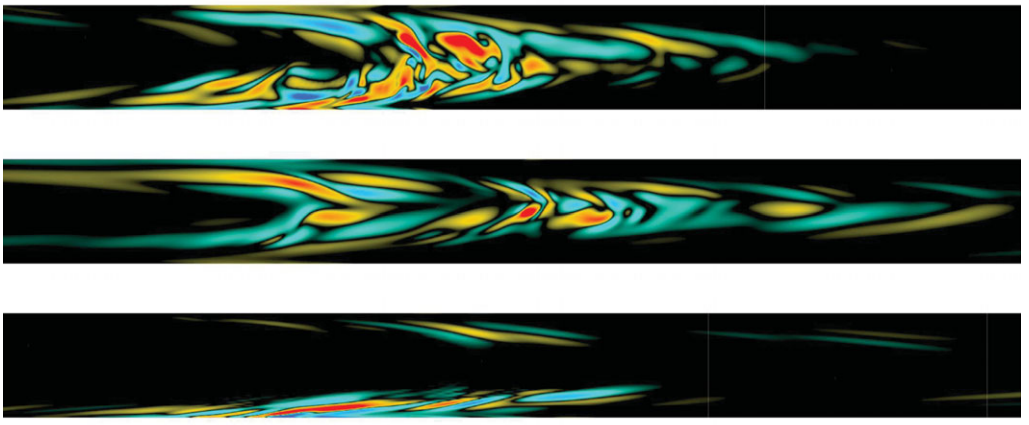


FIGURE 3. (Colour online) (s, z) cut of the axial vorticity field at snapshots on the edge trajectories shown in figure 2 (filled circles). From top to bottom, $Re = 2000$ ($t = 125\ D/U$), $Re = 3000$ ($t = 162.5\ D/U$), $Re = 6000$ ($t = 145\ D/U$). The axial dimension has been scaled by a factor of 2 and only $25D$ of the $33.51D$ computational domain is shown.

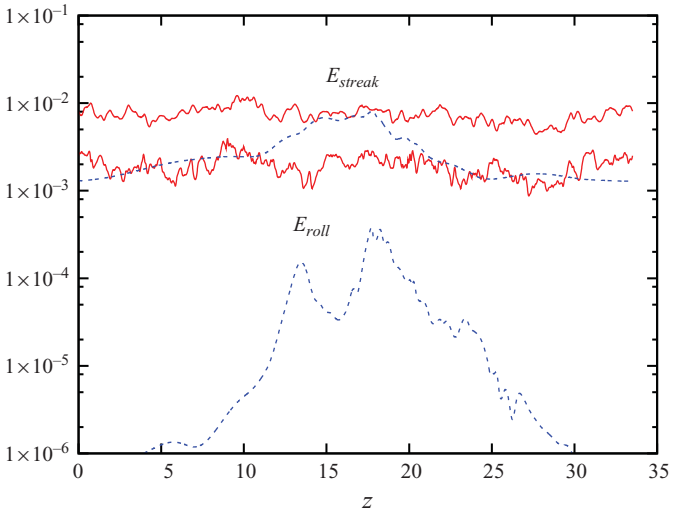


FIGURE 4. (Colour online) The result of an edge calculation at $Re = 3000$ to show localization starting from a globally turbulent initial condition. $E_{roll}(z, t)$ and $E_{streak}(z, t)$ plotted at $t = 0$ (red solid lines) and $t = 84\ D/U$ (blue dashed lines).

turbulence expands spatially once triggered. This edge state localization has already been noted in a $(2 + \epsilon)$-dimensional model of pipe flow (Willis & Kerswell 2009) and, for $Re \leqslant 2800$, in fully resolved computations (Mellibovsky *et al.* 2009). It was observed in a plane Couette flow (Duguet, Schlatter & Henningson 2009; Schneider, Marinc & Eckhardt 2010) as well. Figure 4 confirms that a localized edge state is still reached, even if the starting state for the bisection process is a delocalized turbulent velocity field computed at $Re = 3000$. Figure 4 also shows that the local level of $E_{streak}(z)$ of the edge state in the most energetic region has the same order of magnitude as for the turbulent state, whereas $E_{roll}(z)$ is everywhere at least one decade lower. The plots in figure 3 indicate that the vorticity fluctuations are more

https://doi.org/10.1017/S0022112010003435 Published online by Cambridge University Press

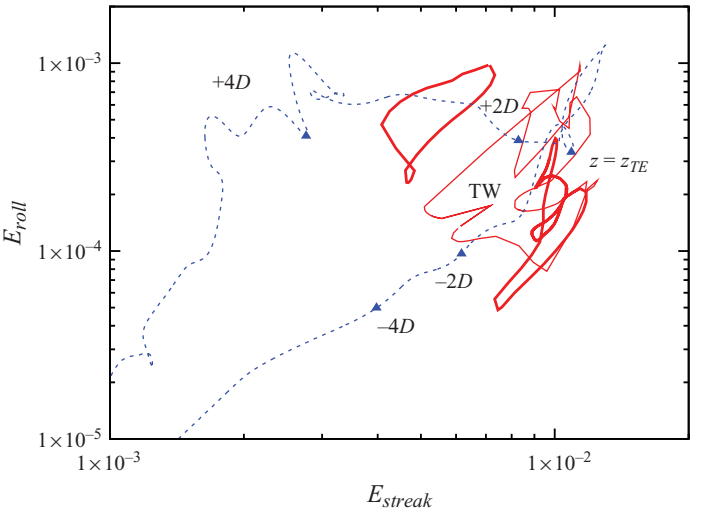


FIGURE 5. (Colour online) Instantaneous phase-space projection on a $(E_{streak}(z), E_{roll}(z))$-plane for $Re = 2000$. Short-domain travelling wave solutions (parametrized by their wavelength α, in red solid lines), edge state (blue dashed lines). The axial coordinate is indicated along the trajectories, along with the position of the trailing edge z_{TE}.

and more exclusively located in the vicinity of the walls as Re increases, culminating for $Re = 6000$ in a radially and azimuthally localized distribution. This is a persistent feature of other edge trackings, after a short transient in which information from the initial state is lost. The implication is clearly that there is an attracting 'edge state' within the edge manifold, as occurs in a short $5D$ pipe, but here, in addition, the edge state is axially localized. Its energy E_{3d} as well as temporal complexity decrease as Re increases. The spatial structure becomes simpler as well in the sense that the edge state is more and more radially localized as Re increases.

The edge state at $Re = 2000$ has a sharp TE and a less abrupt LE so that it resembles a turbulent puff. The heart of the edge state, however, looks less vigorous than that of the puff. This is borne out in the associated perturbation energy which is an order of magnitude lower in the edge state than for the puff. A useful diagnostic for the axial structure of a spatially inhomogeneous flow structure is to project onto the two-dimensional space of (E_{streak}, E_{roll}) (for a puff, see figure 5, Willis & Kerswell 2008). If the structure is axially localized, far upstream and far downstream, both these quantities go to zero as the flow is laminar. Otherwise, the size of the ratio $E_{rolls}/E_{streaks}$ is a good indicator of the underlying dynamics: small values of $\lesssim O(0.05)$ are representative of streak-dominated transitional flows and the host of all exact TW solutions known so far (see, for instance, Pringle *et al.* 2009), whereas $O(0.3)$ values (e.g. the ratio peaks at 0.6 for $z = z_{TE}$ in figure 5, Willis & Kerswell 2008) indicate significantly more cross-stream dynamics, as seen in developed pipe turbulence. Willis & Kerswell (2008) found that the TE region of the puff energetically corresponds to fully developed turbulence, implying the existence of regions upstream and downstream where the flow is transitional. Here the flow associated to the edge state is found to fleetingly resemble the regular arrangement of slow and fast streaks reminiscent of the exact TW solutions. The equivalent plot for the edge state at $Re = 2000$ (figure 5) shows that the TE (indicated by $z = z_{TE}$) has $E_{rolls}/E_{streaks} \approx 0.03$ as opposed to 0.6 for a turbulent puff (Willis & Kerswell 2008) and hence is firmly

https://doi.org/10.1017/S0022112010003435 Published online by Cambridge University Press

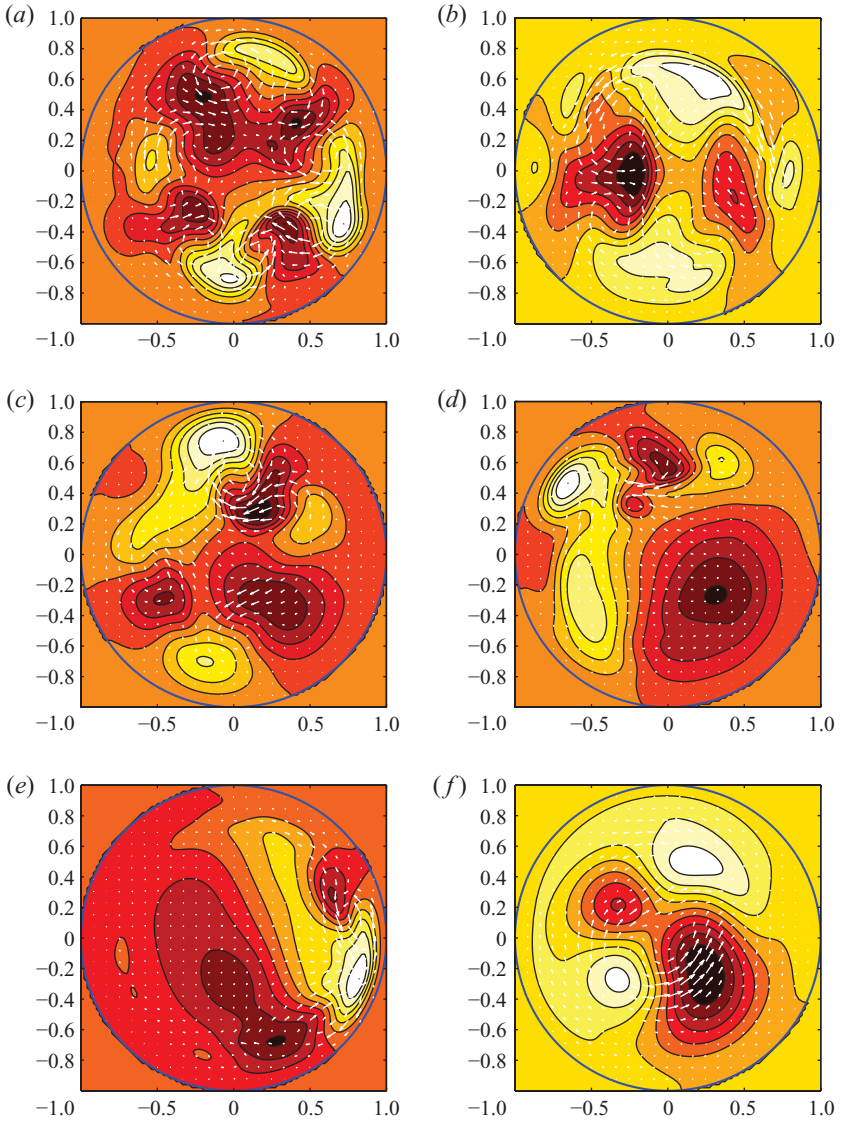


FIGURE 6. (Colour online) Edge states: snapshots of the axial velocity of the perturbation in a cross-section $z = z_{TE}$ located at the trailing edge. The snapshots correspond to low-$E_{3d}(t)$ fields marked by filled and open circles in figure 3 for $t \leqslant 200$ (a,c,e) and $t \geqslant 200$ (b,d,f). (a,b) $Re = 2000$, (c,d) $Re = 3000$ and (e,f) $Re = 6000$. Distances are here in radii $D/2$.

in the transitional regime, as is expected. In fact, for $z = z_{TE} \pm 2D$, there is a striking similarity between the roll and streak energies of the edge state and those of the TWs (of much smaller wavelength and traced out in Kerswell 2005). This match is more than fortuitous. Cross-sectional velocity fields at $z = z_{TE}$, corresponding to the two near-minima of $E_{3d}(t)$ marked with dots in figure 2, are shown in figure 6(a,b). The cross-sectional flow in figure 6(a) has the coherent arrangement of four high-speed streaks near the walls and four low-speed streaks in the core of the flow, while that

https://doi.org/10.1017/S0022112010003435 Published online by Cambridge University Press

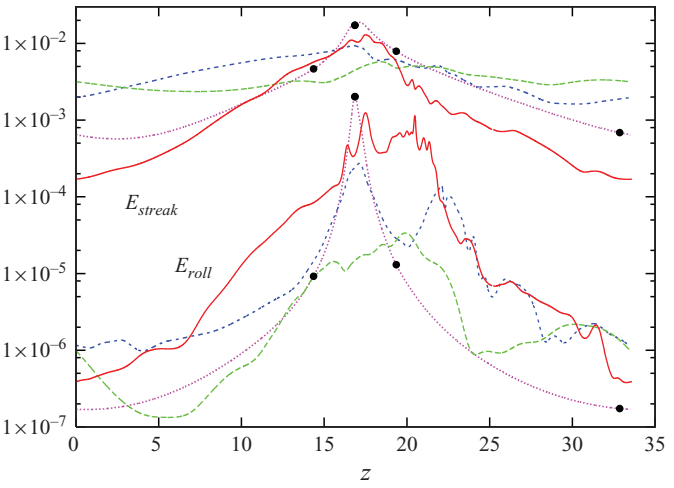


FIGURE 7. (Colour online) $E_{roll}(z)$ and $E_{streak}(z)$ energies for the edge state at $Re = 2000$ (red solid lines) 3000 (blue dashed lines) and $Re = 6000$ (green long-dashed lines). Also shown (magenta dotted lines) are the corresponding quantities (multiplied by 100) for the localized TW found in the $2+\epsilon$ model. Black dots on these curves at 14.3, 16.8, 19.3 and 32.8 indicate the locations of the snapshots shown in figure 10.

in figure 6(*b*) displays an arrangement of two streaks. This suggests two TWs with rotational symmetries of $\boldsymbol{R}_4$ and $\boldsymbol{R}_2$, respectively.

Figure 3 also shows in which sense the spatial structure of the edge state becomes smoother as Re is increased. The strong large-scale fluctuations fill the whole pipe cross-section at $Re = 2000$, but the fraction of the cross-section filled by such fluctuations clearly shrinks from $Re = 2000$ to $Re = 6000$. In the last case (see figure 6*e*), the vorticity of the perturbation seems to be concentrated in the radial and azimuthal directions also, with a predominantly laminar flow near the centreline. Cross-sectional velocity fields for $Re \geqslant 3000$ at the TE ($z = z_{TE}$) (figure 6*c–f*) again show a large degree of coherency with fast and slow streaks appearing together as large-scale structures. The velocity field at $Re = 6000$ is particularly interesting as it looks like a 'minimal coherent state': a pair of streamwise vortices producing a single high-speed streak sandwiched between two low-speed streaks (see figure 6*e*,*f*). This is reminiscent of, but complementary to, a larger-scale structure found in short pipes through edge tracking (Schneider *et al.* 2007*b*; Duguet *et al.* 2008*a*; Mellibovsky & Meseguer 2009) and to the TW S_1 obtained by direct computation (Pringle & Kerswell 2007; Pringle *et al.* 2009). The flow at $t \approx 150$ (in figure 6*e*) has vortices in the opposite sense compared to S_1 – a slow streak is sandwiched between two fast streaks – and remains larger-scale (see e.g. figure 3, Viswanath 2009). The flow at $t \approx 220$ (figure 6*f*) very closely resembles the TW S_1. Figure 7 indicates that the peak axial roll energy decreases more sharply than the corresponding streak energy as Re increases. At all three Re, the edge states travel in the streamwise direction with a time-dependent velocity which is larger than the bulk velocity U.

3.2. *Edge states in reduced symmetry subspaces*

It is natural to ask what form the edge state will ultimately take given that it simplifies in both space and time as Re increases. Taking Re much larger than 6000 proves expensive, with the danger that the bisection algorithm can be misled by numerical instabilities imitating trajectories becoming turbulent. A partial alternative

https://doi.org/10.1017/S0022112010003435 Published online by Cambridge University Press

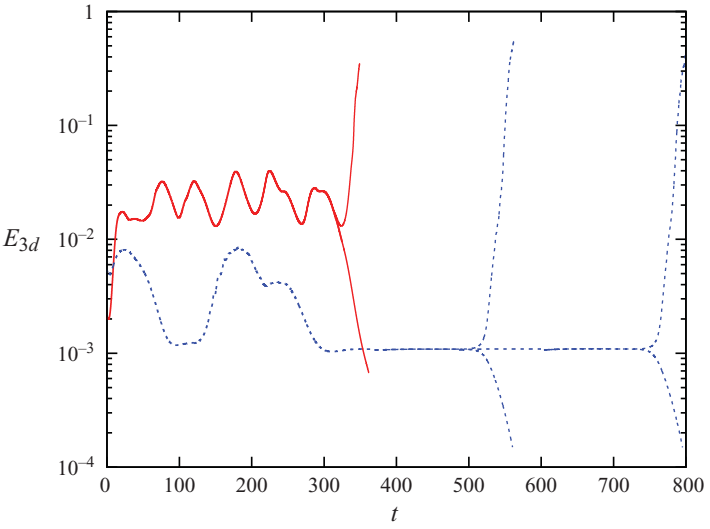


FIGURE 8. (Colour online) $E_{3d}(t)$ during the bisection process at $Re = 8000$ restricted to a $\boldsymbol{R}_3$- and $\boldsymbol{Z}$-symmetric subspace using a resolution $(50, 8, 256)$ (red solid lines) and for the $(2+\epsilon)d$ model ($m_0 = 3$) at $Re = 10^4$ (blue dashed lines).

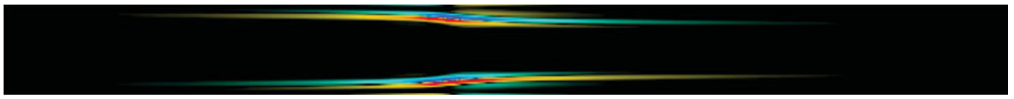


FIGURE 9. (Colour online) Axial vorticity of the localized edge state in the $(2+\epsilon)d$ model: $Re = 10^4$ and $11.2D$ is shown of the $33.51D$ computational domain.

is to restrict the flow dynamics to dynamically consistent subspaces to explore the issue there (Duguet *et al.* 2008*a*). Edge states found in these subspaces are embedded within the 'unrestricted' edge but may not be relative attractors with respect to the full-space dynamics. An edge calculation was performed in an $\boldsymbol{R}_3$- and $\boldsymbol{Z}$-symmetric subspace at $Re = 8000$, using a resolution (50,8,256) (i.e. the azimuthal wavenumbers included are $0, \pm 3, \pm 6, \pm 9, \ldots, \pm 24$). It does indeed show evidence for an edge state with a very low number of active temporal frequencies (see figure 8). The temporal oscillations here suggest the possible existence of relative periodic orbits embedded in a relative attractor on Σ (as a localized counterpart of the orbit found in Duguet, Pringle & Kerswell 2008).

A more severe truncation was also adopted, following the '$2+\epsilon$'-dimensional model of Willis & Kerswell (2009) – which allowed many more computations to be done. This model, which is invoked by choosing a truncation $(N, 1, K)$ (and a value for m_0), is the minimal three-dimensionalization of an axisymmetric simulation, which can qualitatively reproduce the observed flow dynamics in full 3-D (e.g. subcritical transition, localized puffs and expanding slugs). Willis & Kerswell (2009) revealed a localized edge state for the first time (their figure 9) up to $Re \leqslant 4000$. As in that study, $m_0 = 3$ was imposed, corresponding to retaining only the azimuthal Fourier modes $m = -3, 0, 3$ in the simulation. Despite this, the resolution in the radial and axial directions still needs to be high ($N = 35$ and $K = 256$) to reproduce the radial and axial expansions of the turbulent structures, as well as for accurately capturing the steep interfaces expected in slugs. The trade-off of the modelling is a shift in the

https://doi.org/10.1017/S0022112010003435 Published online by Cambridge University Press

values of Re characterizing the appearance of these structures. For instance, whereas puff splitting was observed to occur for $Re \geqslant 2300$ in the fully resolved case, this is delayed to 3200 in $(2+\epsilon)\,d$.

For the $2+\epsilon$ model, the bisection algorithm was run at $Re = 10^4$, where expanding ('global') turbulence is expected. The initial condition, either localized or delocalized, has no influence on the asymptotic edge results, as mentioned in Willis & Kerswell (2009). Figure 8 shows the evolution of $E_{3d}(t)$ during a bisection process. After a transient of duration 300 D/U, the signal $E_{3d}(t)$ on the edge trajectory converges towards a steady value, which stays constant over very large observation times of $O(10^3)$ D/U. This is the signature of convergence towards a relative attractor of constant energy, i.e. a TW solution in the context of a pipe flow. (For analogous plots, see figure 12 in Duguet *et al.* 2008*a* for a pipe flow and figure 1 in Schneider *et al.* 2008 for a plane Couette flow). The phase velocity of the edge state is estimated as $c = (1.06 \pm 0.01)U$, i.e. slightly faster than the bulk velocity. To quantify how well the edge state resembles a TW, the deviation $\delta r(t)$, defined as

$$\delta r(t) = \lim_{\Delta t \to 0} \frac{|\boldsymbol{u}(\boldsymbol{x} - c\Delta t\hat{\boldsymbol{z}}, t + \Delta t) - \boldsymbol{u}(\boldsymbol{x}, t)|}{\Delta t |\boldsymbol{u}(\boldsymbol{x}, t)|}, \tag{3.1}$$

steadily decreased below 10^{-4} as the edge trajectory was tracked. Using the Arnoldi code of Kerswell & Tutty (2007), it was confirmed that this state has only one unstable direction, as expected for an edge attractor.

The spatial structure of the localized edge solution is shown in figure 9, along with the axial distribution of E_{streak} and E_{roll} in figure 7. The axial vorticity is located in a ring-like region of finite radial and axial extents, indicating localization in both senses. Figure 10 shows that the radial concentration is centred on the critical layer at a radius $s \approx 0.69$ consistent with the observed phase speed $c = 1.06U$. At the energy peak, the flow is characterized by a strong azimuthal circulation and a double ring – one inside and one outside the critical layer – of alternating slow and fast streaks. There the streamwise roll pattern undergoes a phase shift of π/m_0 as the critical layer is crossed radially. The presence of the critical layer is less marked $\pm 2.5D$ upstream and downstream, where only one ring of streaks is present. Further away from the heart of the edge state, the cross-sectional velocities are much smaller and the flow becomes almost streamwise-independent. However, the flow is still dominated by a roll and streak patterns, and cannot be confused with a Hagen–Poiseuille flow. The existence of critical layers within lower branch TW solutions in shear flows was mentioned in Wang *et al.* (2007) in the context of a plane Couette flow, and by Viswanath (2009) in the context of a pipe flow. It seems to be a generic property of lower branch solutions when $Re \to \infty$. The streamwise localization is, however, a striking new discovery. Efforts to understand its structure and find similar localized TWs in a three-dimensional pipe flow are currently underway.

3.3. *Summary*

For all values of Re between 2000 and 6000, the spatial structure of the edge state is reminiscent of a turbulent puff with a three-dimensional core region dominated by streaks and streamwise rolls, a sharp arrow-shaped TE interface and a more diffuse LE. As Re is increased, the temporal behaviour of the edge state becomes more regular and the energy concentrates in a narrow region towards the wall so that the central radial region becomes nearly laminar. These trends are particularly exaggerated by the edge state at $Re = 10^4$ in the $(2+\epsilon)\,d$ model introduced by Willis & Kerswell (2009). Here the edge state resembles a localized TW which is steady in a Galilean

https://doi.org/10.1017/S0022112010003435 Published online by Cambridge University Press

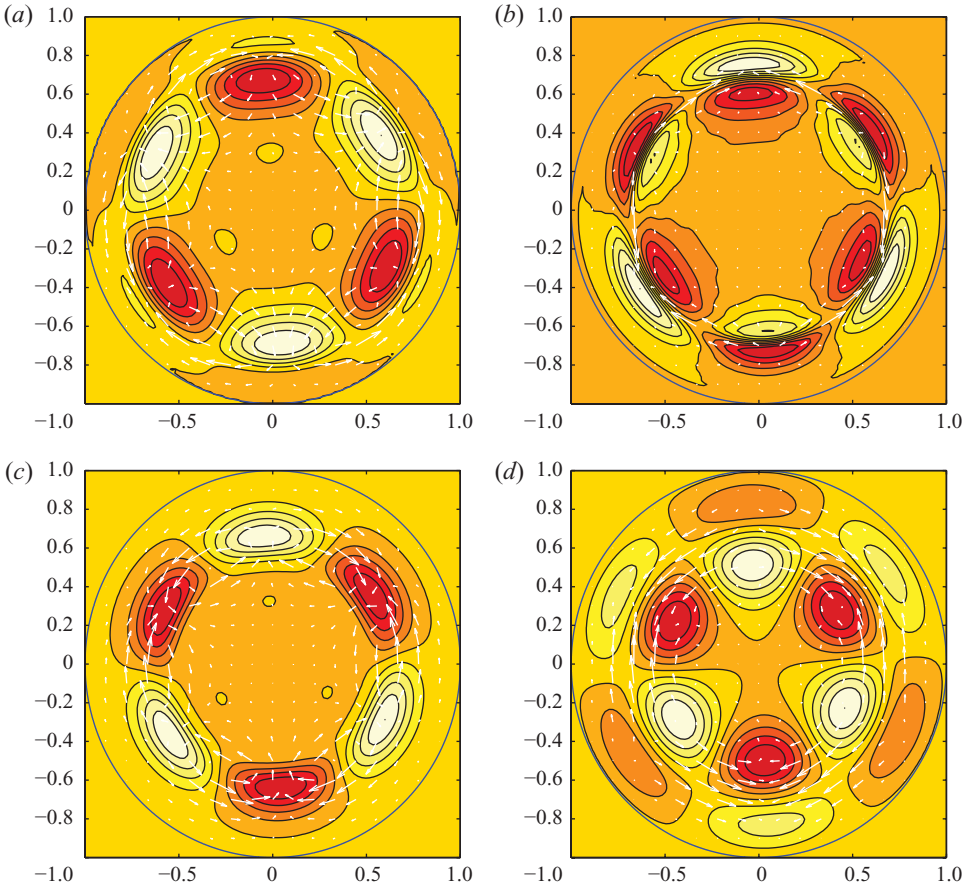


FIGURE 10. (Colour online) The localized edge state in $(2+\epsilon)\,d$ at $Re = 10^4$: velocity field of the perturbation in cross-sections $z = 6.5\,D$ near the TE (a), $z = 9\,D$ in the centre of the active region (b), $z = 11.5\,D$ near the LE (c) and $z = 25\,D$ (d). Contours indicate the axial velocity difference from the laminar flow with the same mass flux (light/dark indicating faster/slower moving fluid) and the arrows represent the cross-stream velocity (length proportional to speed). The amplitude scales are as follows: (a) (cross-stream maximum speed, streamwise maximum speed) $= (1.3 \times 10^{-3}, 3.3 \times 10^{-2})$; ($b$) $(3.1 \times 10^{-2}, 7.3 \times 10^{-2})$; ($c$) $(1.5 \times 10^{-3}, 4.5 \times 10^{-2})$; ($d$) $(1.7 \times 10^{-4}, 1.2 \times 10^{-2})$, all in units of U. Distances are here in radii $D/2$.

frame travelling at $1.06U$. Its spatial structure mimics that of the fully resolved edge state obtained at $Re = 6000$ in being localized in both the radial and axial directions. The localization is, however, more intense, as the energy is concentrated near a ring-like critical layer of finite axial extent, in which the azimuthal shear is relatively intense. This critical layer in the $(2+\epsilon)\,d$ edge state smears out when it is disturbed, evolving into a delocalized turbulent state. Since the edge state is a steady, relative attractor on a hypersurface which is the laminar–turbulent boundary, it only has a one-dimensional unstable manifold. This indicates that the shear instability of the critical layer corresponds to the unstable direction in phase space from the edge state leading to the turbulent state. The flow dynamics corresponding to this unique trajectory in the unstable manifold then represent the purest form of slug genesis for the $(2+\epsilon)\,d$ model. Other initial conditions will approximate this generation, albeit with differences reflecting the precise nature of the starting flow.

https://doi.org/10.1017/S0022112010003435 Published online by Cambridge University Press

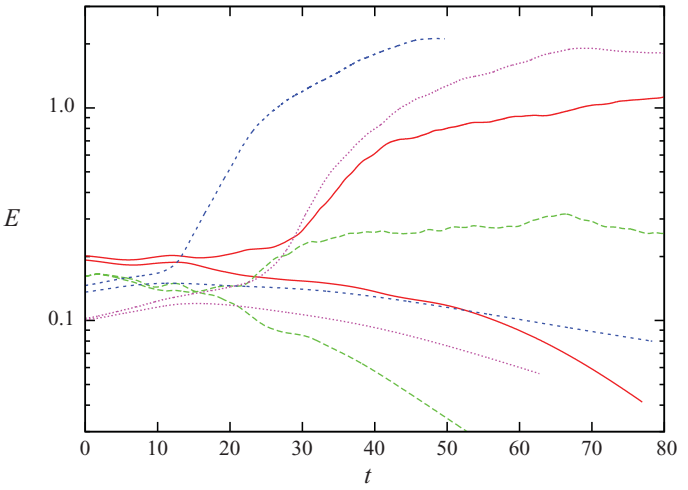


FIGURE 11. (Colour online) Slight perturbations of the perturbation energy $E(t)$, starting from a state on the edge trajectory for a puff, $Re = 2000$ (red solid lines) and the expanding slug $Re = 3000$ (green long-dashed lines), $Re = 4500$ (magenta dotted lines) and $Re = 6000$ (blue dashed lines). Upper trajectories lead to turbulence, while the lower trajectories undergo direct relaminarization.

An extension of this thinking to the fully resolved case is relatively straightforward albeit with a couple of nuances. The first is created by the edge state's apparently complicated temporal dynamics, conjectured to be created by a heteroclinic tangle between various TWs (Duguet *et al.* 2008*a*, *b*). If the edge state has an n-dimensional dynamics (e.g. $n = 0$ for a steady state and $n = 1$ for a periodic orbit), its unstable manifold leading to the turbulent state will be $(n+1)$-dimensional. Trajectories in this manifold are then not formally unique but linked by symmetries of the edge state. It still makes sense to consider any one of these trajectories as defining a characteristic slug evolution for the edge state. The other nuance revolves around whether the edge state is unique or not. Certainly, starting the bisection process off with a variety of different starting conditions leads to what looks to be the same edge state but formally this is difficult to confirm due to its complicated behaviour. Non-uniqueness, however, merely implies that each relative attractor supplies its own route to a globally turbulent state and therefore each has its own corresponding slug evolution. Figure 1 shows a schematic representation of the topology of the neighbourhood of an exact state on Σ. It is close to figure 14 in Duguet *et al.* (2008*a*, *b*), with the notable difference that the edge state corresponds to a localized state, whereas the turbulent state is delocalized. The slug corresponds to an escape of the exact unstable solution (here plotted as a generic saddle point) towards the turbulent state.

4. Slug initiation

In this section, initial conditions close to the edge state are used to study the genesis of a puff at $Re = 2000$ and of slugs at $Re = 3000$, 4500 and 6000. Simulations are started with the initial conditions $\boldsymbol{u}(\boldsymbol{x}, 0) = (1 + \epsilon)\boldsymbol{u}_{edge}$, where $\epsilon = \pm 0.01$ and $\boldsymbol{u}_{edge}$ is a snapshot of the edge state with relatively low E_{3d} (to prolong the evolution phase). Those states have been described in § 3.1, and plotted in figures 3 and 6(b, d, f). In both cases, $\epsilon > 0$ or $\epsilon < 0$, the perturbation energy stays close to that of the edge trajectory for a time of about 10 D/U and then diverges from it (see figure 11).

https://doi.org/10.1017/S0022112010003435 Published online by Cambridge University Press

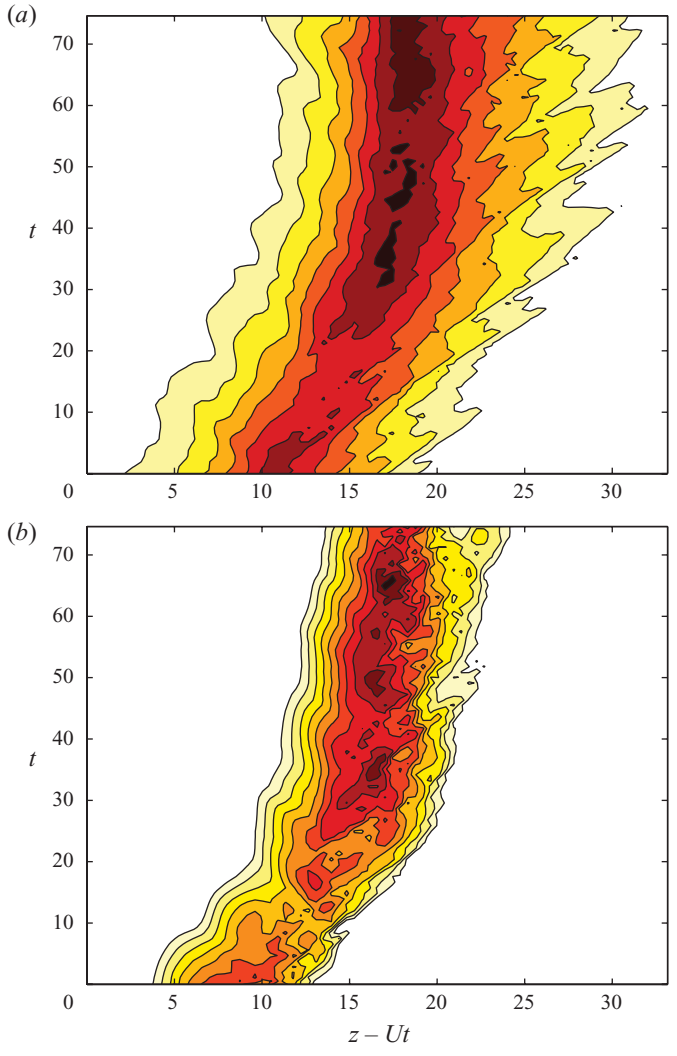


FIGURE 12. (Colour online) Genesis of a puff from the edge state at $Re = 2000$. (a) E_{roll}: scale is $\log_{10}$ from -5 (white) to -1 (black), step 0.5. (b) E_{streak}: scale is $\log_{10}$ from -2.2 (white) to -1.2 (black), step 0.1.

For $\epsilon < 0$, the flow smoothly relaminarizes: the active region loses energy until the flow is dominated by elongated streamwise vortices and streaks which monotonically decay with time. By contrast, for $\epsilon > 0$, the perturbation gains energy and reaches a turbulent state. Those simulations are discussed in the following.

4.1. *Puff genesis at* $Re = 3000$

We first examine the genesis of a turbulent puff at $Re = 2000$, later to be compared to the process of slug genesis. Figure 12 shows $E_{roll}(z, t)$ and $E_{streak}(z, t)$ after the edge state is disturbed at $t = 0$. The flow initially ebbs away slightly in its central region, reaching a low at $t \approx 10$ (recall that all times are in units of D/U) before both energies start to grow back for $t > 20$. This means that the flow stays close to the edge state for $t < 15$, and that only after this period does a puff start to form. By $t = 30$, the core energies have grown to, and stabilized at, larger values than initially.

https://doi.org/10.1017/S0022112010003435 Published online by Cambridge University Press

There is a small deceleration of the TE and an even slower deceleration of the LE, so that the flow structure expands slightly. Both processes stop at $t \approx 50$. At this time, the puff looks fully formed and of stable length, with a velocity very close to the bulk velocity U. The main feature of the evolution is clearly the intensification of the core region, which is consistent with the findings of Mellibovsky *et al.* (2009). The edge state is very similar in shape to the turbulent puff, except in the core energy level, so adjustment is small (e.g. the gradients of E_{roll} are largely constant over time during both the edge and puff stages at either the TE or LE).

Animation of the axial and azimuthal vorticity fields (available online at journals.cambridge.org/flm) in a (s, z)-section shows a steady vortex sheet attached near the pipe wall, upstream of the TE. The vorticity gradient across this vortex sheet is clearly observed to increase in magnitude during the edge → puff transition. Vortices constantly roll up on top of the vortex sheet, forming wavepackets propagating downstream faster than the turbulent puff (Shimizu & Kida 2009). These vortical structures had already been pointed out in experiments by Bandyopadhyay (1986). They are qualitatively and quantitatively very reminiscent of the early stage of the Kelvin–Helmholtz (KH) instability for a two-dimensional vortex sheet.

4.2. *Slug genesis at* $Re = 3000$

At $Re = 3000$, once away from the edge state, the evolution differs strongly from the $Re = 2000$ case. Figure 13 shows that the flow initially ($t \approx 5$) starts to change with a core intensification of E_{roll} reminiscent of puff formation. This is followed by a sudden deceleration of the TE ($t \gtrsim 10$), as indicated by E_{roll}, a feature which is absent in the $Re = 2000$ case. The main evolutionary stage is the interval $20 < t < 40$, when the core region immediately downstream of the TE sees steadily increasing gradients in both roll and streak energies. This leads by $t \approx 35$ to high energies downstream and in the centre of the evolving structure. At $t = 40$, the roll energy has stabilized at a high level at the centre of the slug while its axial gradients are slowly weakening at the LE. For $t > 40$, local maxima of E_{roll} and E_{streak} are both to be found near the TE. Downstream of the TE, the average level of E_{streak} is comparable to the level in the active region of the edge state, while E_{roll} is everywhere larger than its edge counterpart.

During the escape from the edge state, the propagation speed of the TE, c_{TE}, drops from the initial value of $1.40U$ (the speed of the edge state) to $0.84U$. In contrast, the speed of the LE, c_{LE}, decreases slowly from $1.40U$ to approximatively $1.18U$ by the end of the simulation. Experimental measurements by Lindgren (1969) at $Re = 3000$ suggest that $c_{LE} = 1.13U$ and $c_{TE} = 0.83U$. This is confirmed by later experiments by Wygnansky & Champagne (1973), Hof *et al.* (2005) and Nishi *et al.* (2008), and compares favourably with the present numerical measurements. Note that even after $t = 40$, the iso-contours of E_{roll} near the LE do not form a straight line in the $(z - Ut, t)$ diagram of figure 13. This suggests that the slug expansion at $Re = 3000$ is not strictly continuous but occurs by jumps, as pointed out in the experiments by Lindgren (1969) 'just above the threshold for transition'.

The axial vorticity is shown in a series of snapshots across the period $t = 10$–40 in figure 14. As for $Re = 2000$, vortical structures located on the vortex sheet behind the TE start to grow in amplitude at $t = 25$ on top of the vortex sheet. In their initial stage, these vortical structures are again very reminiscent of the rolling-up vortex sheet observed in the early stage of the KH instability. The presence of roll-up fluctuations is also evident in figure 15 at $Re = 4500$. While, for $Re = 2000$, these fluctuations catch up with the active region, here some of the vortices stay initially

https://doi.org/10.1017/S0022112010003435 Published online by Cambridge University Press

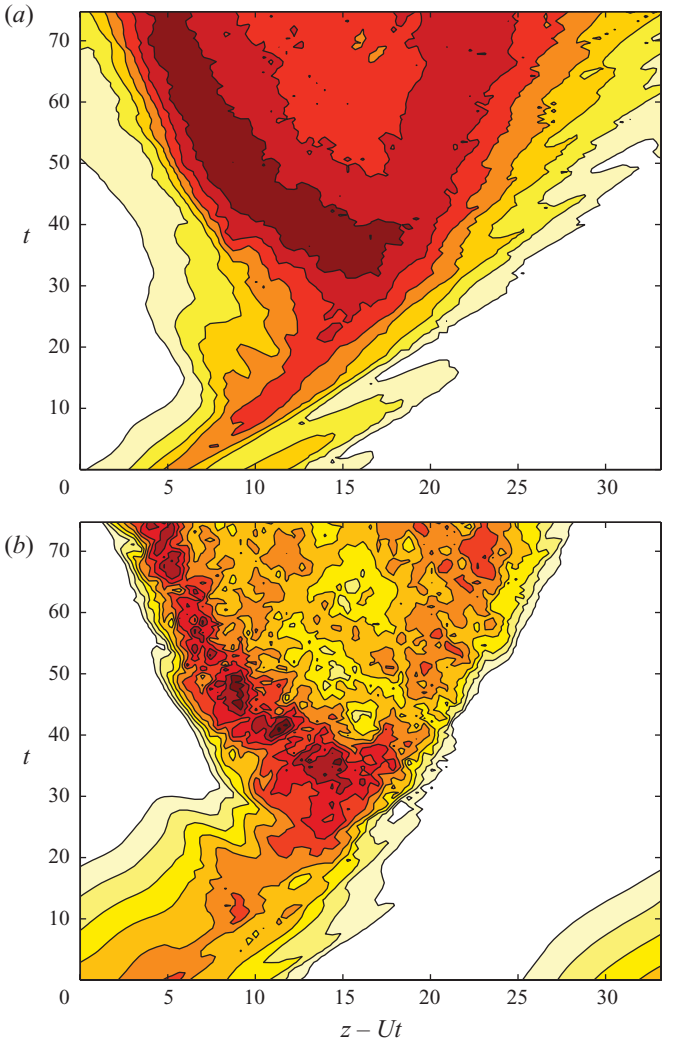


FIGURE 13. (Colour online) Genesis of a slug from the edge state at $Re = 3000$. (*a*) E_{roll} and (*b*) E_{streak} (scales as in figure 12).

in the laminar zone just upstream of the active region, as a sign that they actually travel at a slower velocity. During the later stage of their evolution, the vortices are frequently ejected from the vortex sheet, with no sign of clear temporal periodicity, and migrate towards the centreline. In the latest stage of their evolution, the vortices break down, generating a new turbulent motion which rapidly fills the laminar zone located directly upstream of the TE interface and surrounded by the vortex sheet. As a consequence, the TE interface delimiting the laminar flow from the turbulent flow has moved upstream relative to the turbulent zone. Meanwhile, the dynamics at the LE and its propagation has stayed unchanged. This results in a streamwise elongation of the active region, whose origin is clearly the shear instability near the TE. The global elongation of the turbulent structure results from a sequence of such repeated vortex ejection events (see video online).

https://doi.org/10.1017/S0022112010003435 Published online by Cambridge University Press

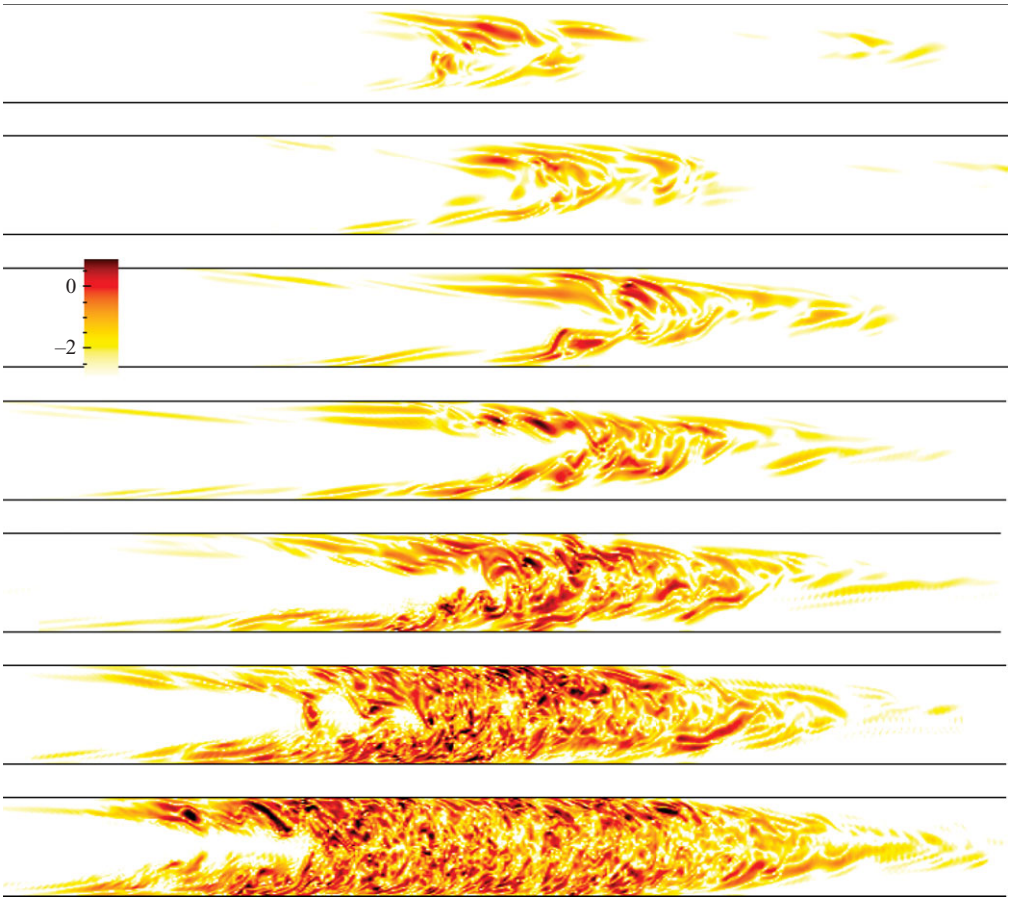


FIGURE 14. (Colour online) Axial vorticity for the edge-to-slug evolution shown in figure 13, $Re = 3000$ (top to bottom, $t = 10, 15, 20, 25, 30, 35, 40\ \ D/U$). Top colourbar indicates $\log_{10}$ values.

The interfaces, though very unsteady, are best described by a long arrow-shaped LE, clearly detached from the wall, and a sharp concave TE. While the strongest vorticity is located dominantly at the TE, and to a lesser extent, near the LE, a more quiescent region forms in the core. The vorticity and the roll energy in this central region occasionally reach low local values, close to that of the laminar flow, suggesting that the localized structure is close to splitting into two (see E_{roll} in figure 13), which is actually observed experimentally for slightly lower values of Re.

4.3. *Slug genesis at* $Re = 4500$ *and* 6000

Slug genesis at $Re = 4500$ and 6000 consists of the same phases as for $Re = 3000$; however, the duration of events is considerably shortened. The corresponding space–time diagrams are, respectively, displayed in figures 16 and 17. Focusing here on $Re = 6000$, the intensification of E_{roll} within the core of the edge state starts at $t \approx 9$, quickly followed by the intensification of E_{streak} at $t \approx 12$. The intensification of energy gradients at the TE is faster than that at 3000, being largely over by $t = 20$ compared to $t = 40$ there. Similarly the time for the slug to fill the (computational) pipe is $\approx$35 rather than 50 at 3000. Interpolation of the final front velocities from E_{roll} in figure 17 yields $c_{TE} = 1.58U$ and $c_{LE} = 0.56U$ at $Re = 6000$. Similar interpolation

https://doi.org/10.1017/S0022112010003435 Published online by Cambridge University Press

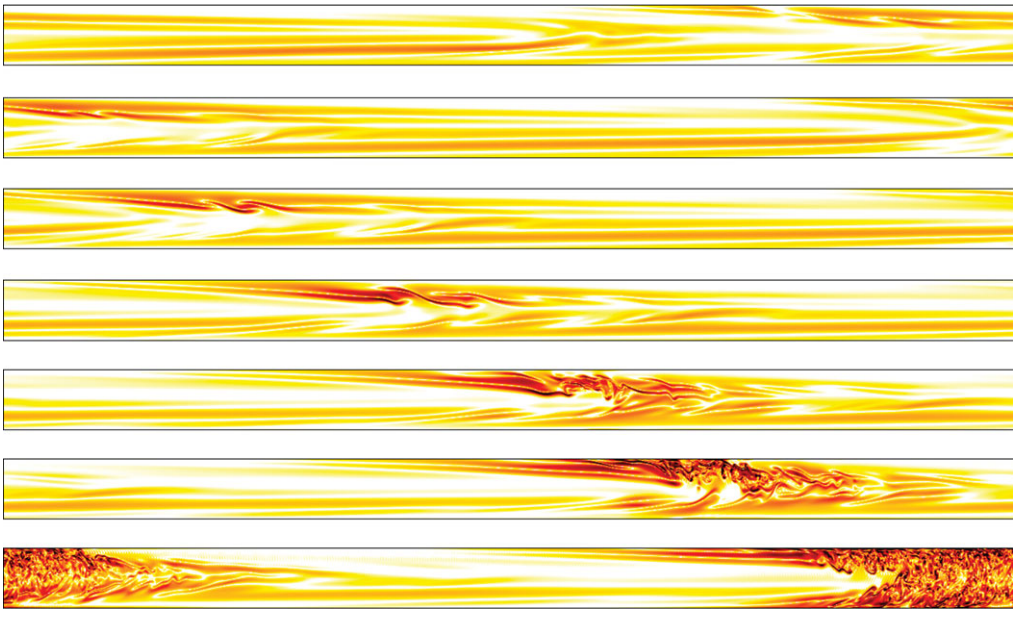


FIGURE 15. (Colour online) Azimuthal vorticity focusing on the instability of the edge state leading to the early formation of a slug, as shown in figure 16, $Re = 4500$ (top to bottom, $t = 5, 12.5, 15.75, 20.3, 25, 27.5, 35.25\ \ D/U$) (same scale as in figure 14). Animation available online.

from figure 16 yields $c_{TE} = 1.47U$ and $c_{LE} = 0.68U$ at $Re = 4500$. This is in very good agreement with experimental estimates, given the difficulty in measuring the speed of the LE experimentally. However, the most striking feature of the E_{roll} and E_{streak} evolution plots is now the large gradient of E_{roll} at the LE. This is consistent with experimental observations, but is nevertheless eye-catching compared to the more diffuse LE for $Re = 2000$ and 3000.

A typical sequence of plots visually representative of the elongation mechanism of the slug is shown in figure 18 for $Re = 4500$. The quantity displayed is the azimuthal vorticity of the perturbation to the base flow. As for $Re = 3000$, intense vortical structures start to develop near the vortex sheet behind the TE. Again, these vortical structures clearly resemble a rolling-up vortex sheet observed in the early stage of the KH instability. Their propagation velocity is initially slower than the overall speed of the turbulent region from which it originates, thus inducing a time delay: the vortical fluctuations are left behind the passing slug. The destabilization of these vortical fluctuations results in an ejection process, leading to the formation a local blob of turbulence. Initially this blob is clearly distinct from the turbulence in the active region already developed at earlier times; however, its vortical intensity becomes quickly comparable to the levels observed at the TE. This localized blob of turbulence migrates towards the centreline, invading the whole cross-section of the pipe. Immediately after it aggregates to the existing slug. The global elongation of the turbulent structure apparently results from an intermittent sequence of such repeated ejection $\rightarrow$ destabilization $\rightarrow$ aggregation events (see video online).

For $Re = 6000$, the azimuthal vorticity of the perturbation to the base flow is shown in figure 19. Just like the evolution at $Re = 3000$ and 4500, the flow departs from the edge state through a clear roll-up of the vortex sheet at $t \approx 12$. However, the

https://doi.org/10.1017/S0022112010003435 Published online by Cambridge University Press

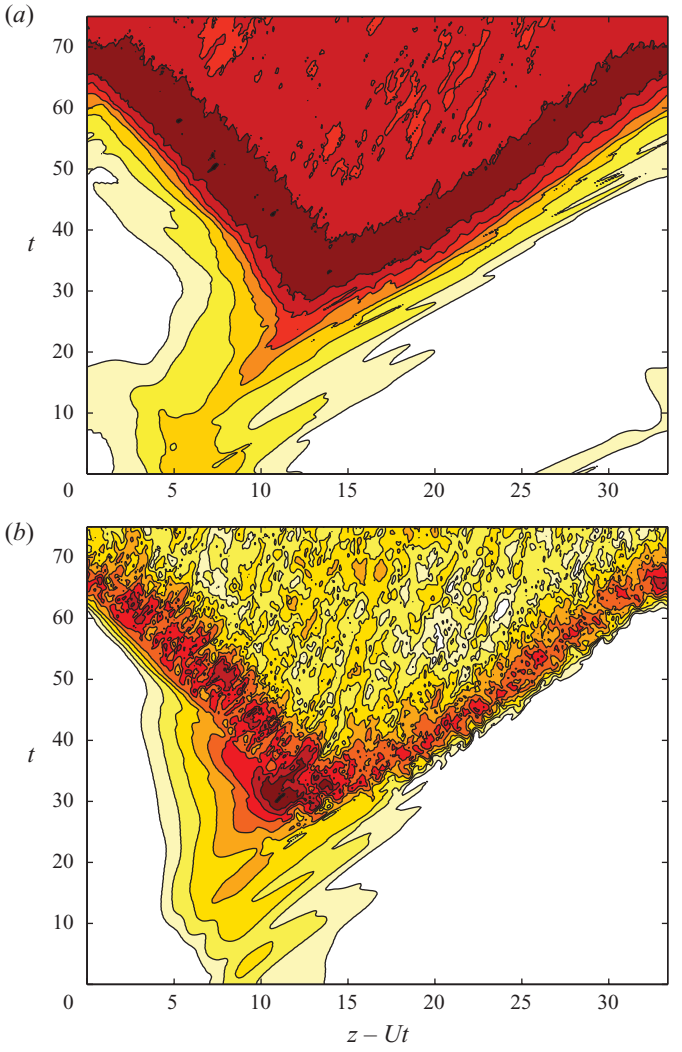


FIGURE 16. (Colour online) Genesis of slug from the edge state at $Re = 4500$. (*a*) E_{roll} and (*b*) E_{streak} (scales as in figure 12). The resolution is (60, 48, 384).

vortical motion associated to the edge state at $Re = 6000$ was shown in figure 6 to be off-centred and predominantly located in one angular sector near the pipe wall. Consequently, its linear instability phase (intensification of the vorticity gradients across the vortex sheet), as well as the nonlinear phase (roll-up and destabilization of the vortex sheet) are also very localized near that wall. Visualizing the vorticity in an (s, z)-plane again reveals the repeated formation of KH vortices. This calls for a detailed study of the dynamical evolution of these coherent structures, and an exploration of their possible relation to hairpin vortices (see, for instance, Adrian 2007). The average size of these vortices appears smaller than those found at $Re = 3000$. These vortices instantaneously break down to generate a localized pocket of turbulence near the wall, visually analogous to the formation of spots in flat boundary layers. As the roll-up process repeats itself over time, turbulent motions invade the pipe not only in the axial direction but also azimuthally, until the whole

https://doi.org/10.1017/S0022112010003435 Published online by Cambridge University Press

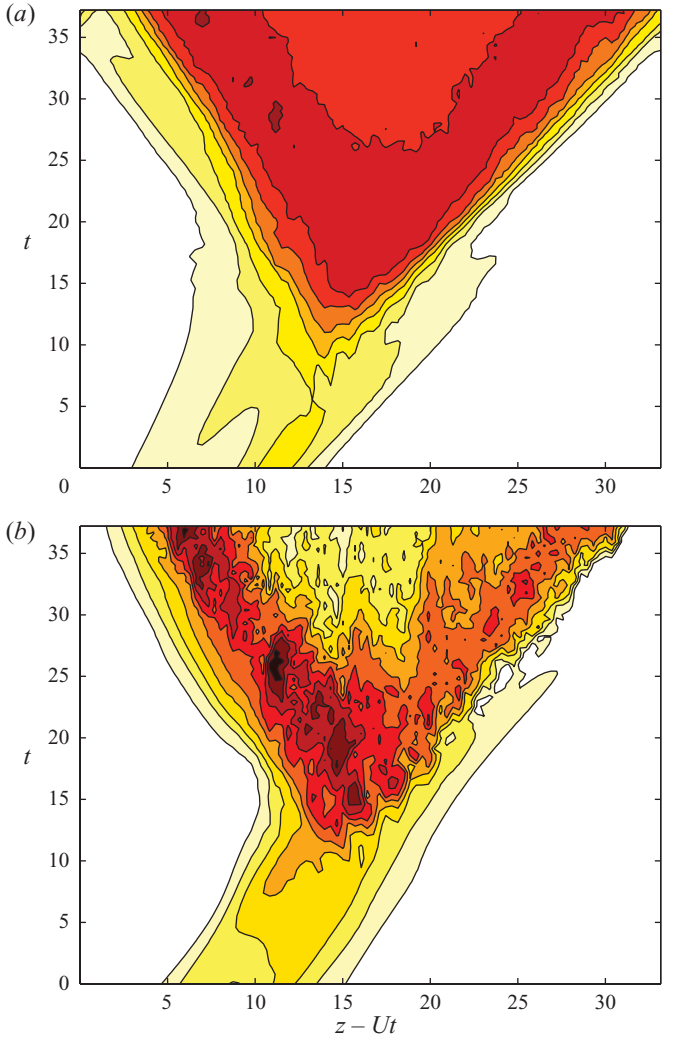


FIGURE 17. (Colour online) Genesis of slug from the edge state at $Re = 6000$. (*a*) E_{roll} and (*b*) E_{streak} (scales as in figure 12). The resolution is (60, 48, 384).

cross-section is filled at around $t \approx 20$. The expanding slug eventually takes a neat cylindrical shape with arrow-shaped ends, analogous to the $Re = 3000$ case, but with considerably smaller internal scales. Ejection of KH vortices is also evident near the LE, and though present, to a lower extent, throughout the flow it is obscured by multiple events. This is consistent with figure 17 and with the fact that strong gradients of E_{roll} also occur at the LE, compared to the $Re = 3000$ case where only the TE can trigger strong vorticity fluctuations.

4.4. *Vortical fluctuations*

Shimizu & Kida (2009) have analysed the propagation of these vortical disturbances for a turbulent puff and suggested a cyclic mechanism responsible for its sustenance. The vortex sheet at the TE consists of low-speed fluid induced by the turbulent motion near the wall and left behind the puff. It becomes unstable and triggers three-dimensional vortices. Their study suggests that the ejection of KH vortices, resulting

https://doi.org/10.1017/S0022112010003435 Published online by Cambridge University Press

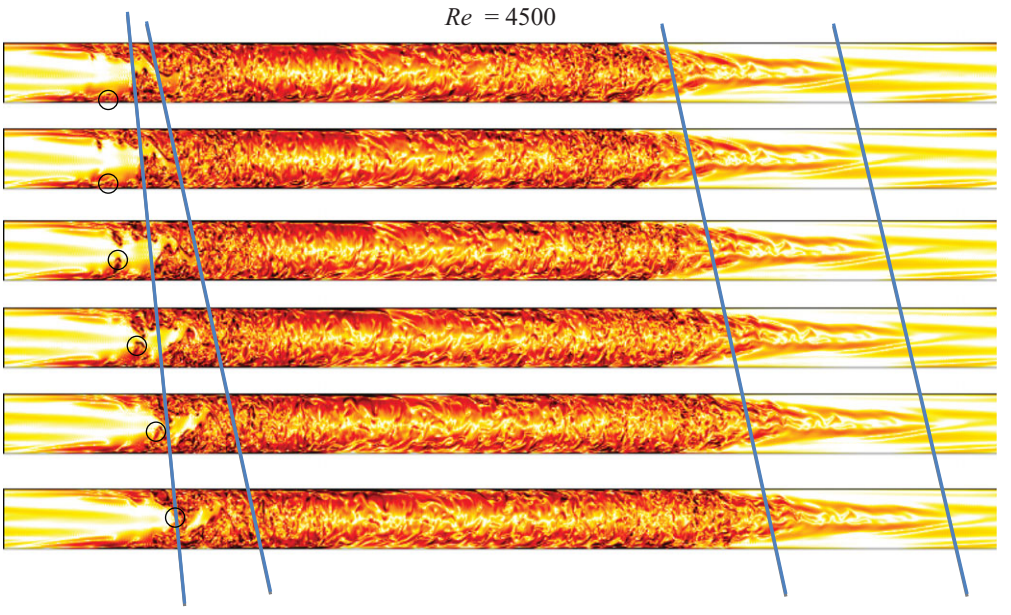


FIGURE 18. (Colour online) Azimuthal vorticity perturbation during slug expansion at $Re = 4500$, focusing on one single ejection event upstream of the TE (top to bottom; $t = 47.85$, 48.05, 48.55, 49.05, 49.55, $49.85\, D/U$) (same scale as in figure 14). Open circles are drawn in order to facilitate the visual identification of ejected KH vortices, as in the vortex tracking method. Three parallel lines are drawn schematically as guidelines for the LE velocity $\dot{z} = c_{LE}$, another line symbolizing the TE velocity $\dot{z} = c_{TE}$. Animation available online.

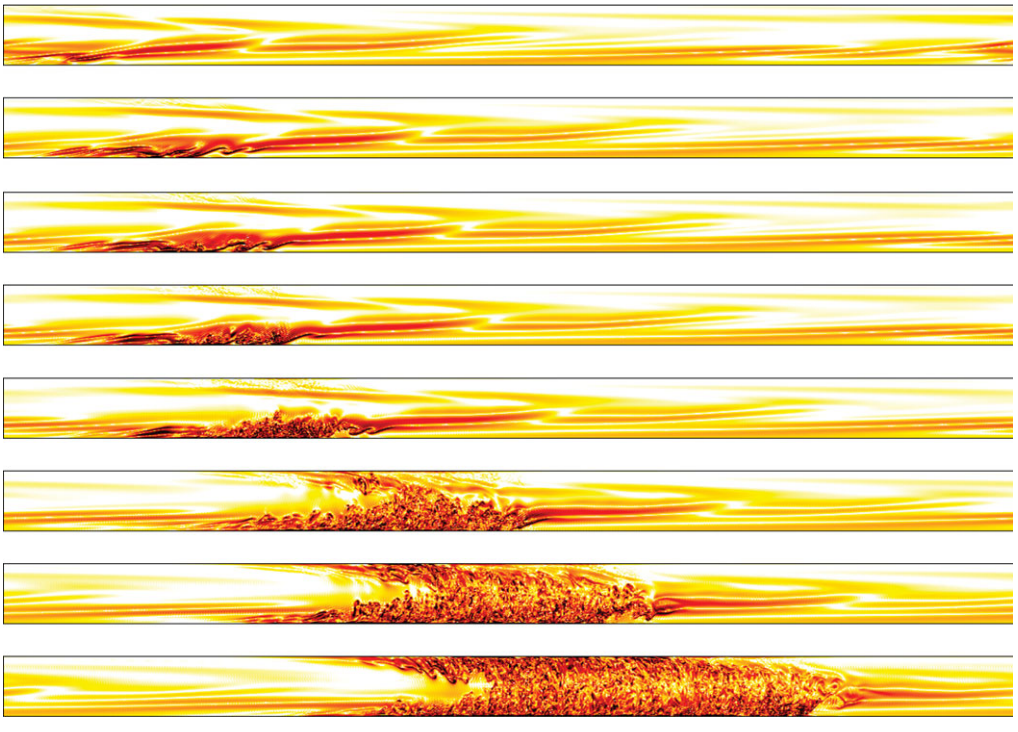


FIGURE 19. (Colour online) Azimuthal vorticity perturbation for the edge-to-slug evolution shown in figure 17, $Re = 6000$. (top to bottom, $t = 9.536$, 12.522, 13.268, 13.783, 16.065, 18.235, $20.727\, D/U$) (same scale as in figure 14). Animation available online.

https://doi.org/10.1017/S0022112010003435 Published online by Cambridge University Press

from the large gradients across the vortex sheet, plays a key role in the sustenance mechanism of the turbulent puff: these vortices propagate downstream with a velocity greater than that of the puff; hence, they represent the missing link to feed turbulent fluctuations back into the turbulent puff. The loop is plausibly closed because the KH fluctuations travel at a phase velocity faster than that of the puff itself.

We now wish to investigate how this mechanism is altered when turbulent puffs are no longer equilibrium states. Vortical structures growing on top of the vortex sheet near the TE are also detected by eye in figures 14, 18 and 19. Animation of the case $Re = 6000$ (expanding slug) clearly shows that all fluctuations ejected from the TE interface travel slower than the vortex sheet from which they originate. In contrast, at $Re = 2226$ in Shimizu's data (localized puff), the KH fluctuations are faster than the puff at least in the radial region between the pipe axis and the vortex sheet. Given this, we focus here on the axial propagation speed of the vortical structures and compare it with the corresponding speed of the turbulence as Re varies. The main idea here is that the value of c_{TE} (to be compared eventually to c_{LE}) is controlled solely by the vortex dynamics at the TE, which in turns depends on both the initial vortex propagation speed C_{KH} and a representative speed of the turbulence. Since in a developed slug both interfaces travel at different velocities, the question arises which quantity should be taken as a reference velocity of the bulk turbulence. From figures 13, 16 and 17 as well as from the animations online, it is clear that the sudden deceleration of the TE is responsible for the elongation, and that the instability mechanisms acting during the edge $\rightarrow$ slug evolution act at the upstream interface. On the contrary, the LE behaves as a passive region connecting the turbulent zone to the laminar downstream of it. It is characterized by a front propagation speed c_{LE}, which appears to be dependent only on Re, independently of whether there is a upstream interface and of the possible dynamics occurring there. For instance, in a high-Re experimental pipe set-up where disturbances would be injected continuously near the inlet, a propagating front delimiting the turbulence and the laminar flow would plausibly travel downstream at the same velocity c_{LE}, whereas in that case there is no such thing as a TE. It thus appears natural, at a given value of Re, to regard c_{LE} as the propagation speed of the turbulence through a laminar environment. Note that understanding the experimentally observed dependence of c_{LE} on Re is an open issue, whose determination undoubtedly necessitates full knowledge of the distribution of the Reynolds stresses inside the turbulent zone. Rationalizing this is beyond the scope of the present investigation. Instead, c_{LE} as an observed function of Re is adopted here as a representative of the speed of the turbulence as a whole.

The method used to track each individual KH vortex is relatively simple: the location of localized maxima of the azimuthal vorticity perturbation ω_θ is tracked against time in a given (s, z)-section. The axial velocity C_{KH} of each ejected vortex is then interpolated numerically by a linear fit. This method relies on an unambiguous identification of intense peaks of ω_θ in the chosen plane. Such a condition is not fulfilled in practice for all vortex events, for instance, if the chosen vortex drifts away from the chosen (s, z)-plane, or if the location of the maximum is too patchy to be accurately tracked. The number of in-plane vortices which can be accurately tracked in our videos (available online) is $O(15)$, which appears just sufficient to get useful statistics. The axial velocity of all tracked vortices is shown in figure 20 against their radial position for $Re = 2000$, 3000, 4500 and 6000. The spread in the data necessarily calls for a statistical description of the process. All perturbations have their maximum located between $s = 0$ and $s = 0.28$ (in units of D). Their instantaneous axial velocity lies between U and $2U$ (respectively the puff velocity and the centreline velocity

https://doi.org/10.1017/S0022112010003435 Published online by Cambridge University Press

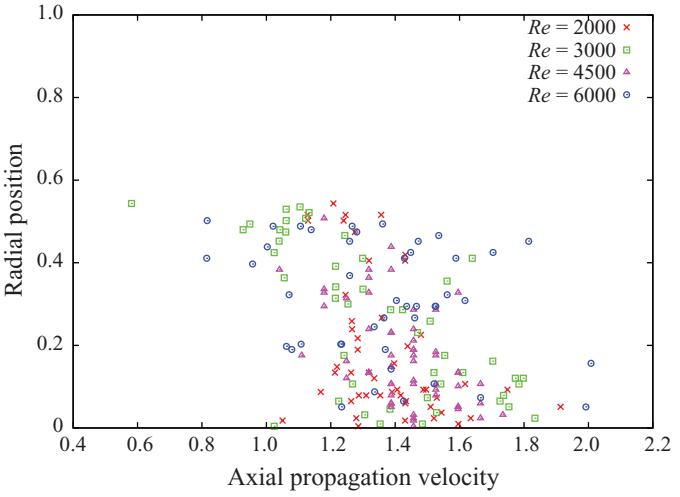


FIGURE 20. (Colour online) Axial velocity of the KH vortices as a function of their radial position (here in units of the radius $D/2$), for $Re = 2000$, 3000, 4500 and 6000.

of the laminar flow) at $Re = 2000$. For $Re \geqslant 3000$, it lies between $0.6U$ and $2U$. Importantly, the distribution of C_{KH} resembles neither the laminar parabolic profile nor the turbulent one, which suggests that we are not trivially measuring the passive advection of perturbations by the flow.

The axial velocity C_{KH} in the database was averaged over the whole vortex population for each value of Re. The mean value $\langle C_{KH} \rangle$ varies with Re between 1.34 and 1.38, which essentially suggests that $\langle C_{KH} \rangle$ is independent of Re, as should be expected for the suspected underlying inviscid KH mechanism. For comparison, we have also used the data in figure 14 by Shimizu & Kida (2009), which corresponds in our units to a flux-based Reynolds number of $Re = 2226$ in a smaller pipe of length $L = 25.13D$. Those authors track the velocity $U_f(s, z)$ of perturbations by measuring space–time correlations, and compare it to the puff velocity. The perturbations they also identify with KH structures are located in the central region $|s| \leqslant 0.3$, for which the z-averaged quantity $\langle U_f \rangle_z(r)$ varies between $1.15U$ and $1.35U$. Despite a different tracking algorithm, we consider this correspondence reassuring, especially given the difference in pipe lengths and the possible influence of a shorter pipe on the puff dynamics.

We now compare the propagation velocity of the KH vortices to the velocity c_{LE} and c_{TE} of the LE and the TE (respectively), deduced by interpolation from figures 12, 13, 16 and 17 . Our values of c_{LE} and c_{TE} are shown in figure 21 as a function of Re. They compare very well with available experimental data by Lindgren (1969), Wygnanski & Champagne (1973), Hof *et al.* (2005) and Nishi *et al.* (2008). Adding now the data for the average speed $\langle C_{KH} \rangle$, the average speed plus or minus the standard deviation $\langle C_{KH} \rangle \pm \delta C_{KH}$, and the minimum value $\min C_{KH}$ as functions of Re in figure 21, a clear trend is noticeable which we summarize as follows.

(i) For $Re = 2000$, $c_{LE} = c_{TE} \approx 1.03U$, much below $\langle C_{KH} \rangle - \delta C_{KH} = 1.26U$ and below $\min C_{KH} = 1.05U$. This is the case where turbulence stays localized inside a turbulent puff structure. As can also be seen from figure 21, all vortices travel faster than the turbulent puff.

(ii) For $Re = 3000$, $c_{LE} \approx 1.16U$, below $\langle C_{KH} \rangle$ but slightly above $\langle C_{KH} \rangle - \delta C_{KH}$ and clearly above $\min C_{KH} = 0.93U$. (Note that we have omitted the possible rogue data

https://doi.org/10.1017/S0022112010003435 Published online by Cambridge University Press

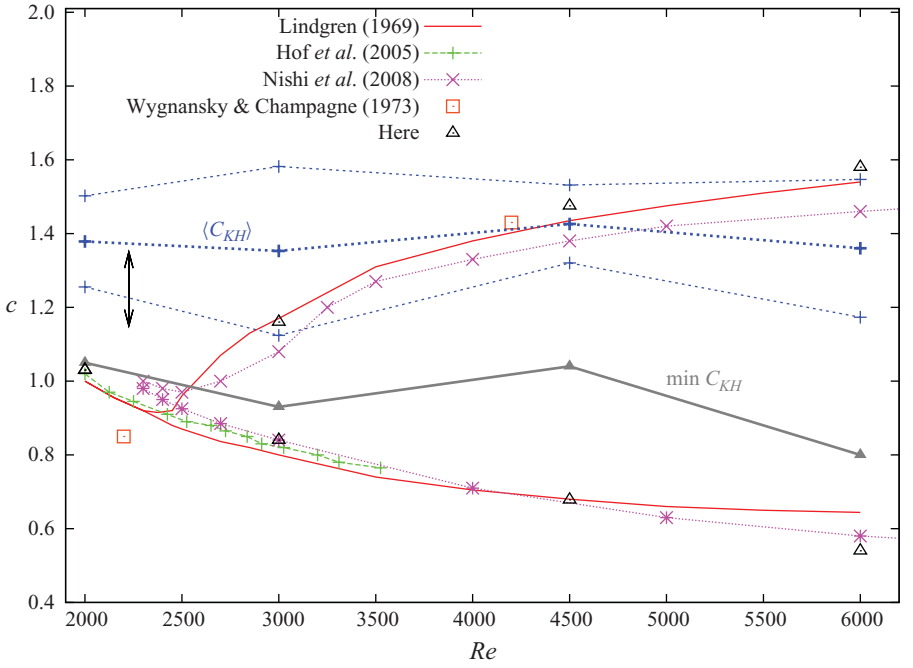


FIGURE 21. (Colour online) Axial velocity of the LE and the TE as a function of Re (triangles), compared with available experimental data. The velocity of the LE is always greater (slugs) or equal (puffs) to that of the TE. The mean axial propagation velocity $\langle C_{KH} \rangle$ of KH vortical structures ejected from the TE is indicated, plus or minus its standard deviation δC_{KH} (see § 3.4), as well as the minimum value $\min C_{KH}$ among the data at hand. The arrow at $Re = 2226$ indicates the statistical velocity of fluctuations computed by Shimizu & Kida (2009).

point $C_{KH} = 0.58U$ present in figure 20, which would only exaggerate the trend.) This is a slug case where turbulence expands discontinuously through the pipe. According to the statistical description, we note that some of the vortices (the slowest ones) do not catch up with the LE velocity.

(iii) For $Re = 4500$ and even more clearly for $Re = 6000$, c_{LE} is above $\langle C_{KH} \rangle$, close to $\langle C_{KH} \rangle + \delta C_{KH}$ and much above $\min C_{KH}$. This is a case of continuous slug expansion. Statistically, almost all vortices propagate at a velocity slower than the bulk turbulence.

The interpretation is straightforward: the turbulent state stays localized as long as all KH vortices travel faster than the LE. Otherwise, it delocalizes, expanding spatially by accretion when at least some of the vortices do not catch up with it. Our analysis for the puff case confirms the observation made by Shimizu & Kida (2009): all KH vortices travel faster than the turbulent puff. In the slug case, the sequence of events shown in figure 18 is entirely representative of the dynamics shown in the online videos for $Re = 3000$, 4500 and $Re = 6000$: slow KH vortices are ejected towards the centreline, break down in the wake of the turbulent state travelling faster downstream. The original turbulence then elongates through accretion. The process repeats itself until a turbulent flow has invaded the whole pipe. According to figure 21, for larger Re, the likelihood of a given KH vortex catching up with the turbulent structures decreases and the slug expansion can truly be described as continuous

https://doi.org/10.1017/S0022112010003435 Published online by Cambridge University Press

when (statistically) all vortices contribute through their early breakdown to the axial expansion of the slug.

5. Discussion

This paper has examined the likely route through which turbulent slugs are generated by focusing on how the relative attractor (the edge state) on the laminar–turbulent boundary breaks down. If the edge state is unique, this can be viewed in some sense as the generic situation, since, for all but the most drastic initial perturbations, the disturbed flow will, at least initially, evolve towards the edge state before being directed away by its unstable manifold. As a result, experiments working with disturbances just above the transitional threshold should see essentially this slug genesis. The flow development along the unstable manifold of the edge state is also a natural way of defining a slug since it is a constantly expanding, evolving state.

For all values of Re examined so far (1800–2800 in Mellibovsky *et al.* 2009 and up to 6000 here), these edge states are always found to be axially localized despite the fact that the associated turbulent state delocalizes beyond ≈ 2300. They appear to have chaotic dynamics and look very similar to puffs albeit with less energy especially in their core (Mellibovsky *et al.* 2009; Willis & Kerswell 2009). Their internal dynamics are found to smoothen temporally and become even more localized spatially with increasing Re, reflecting the fact that the edge state approaches the laminar rather than the turbulent state energetically. Working within symmetric subspaces exaggerates this trend by revealing an almost periodic state and, in $2+\epsilon d$, the simplest state possible, which appears to be a TW.

Once the edge state is weakly perturbed at $Re \geqslant 3000$, slug genesis is observed to occur through three distinct phases:

(i) intensification of the core energy and subsequent front sharpening,

(ii) shear instability of the wall-attached vortex layer set-up at the TE,

(iii) spatial expansion through the contamination of the fluid left behind the TE.

The first two phases are also seen during puff genesis at $Re = 2000$. In particular, at all Re studied, the instability of the edge state manifests itself initially by a local increase of energy and sharper velocity gradients at the TE which form an intense vortex sheet near the wall at the TE. This shear is unstable to what looks to be a KH instability and rolled-up vortices are shed (see, for instance, figure 15). These travel downstream at a Re-independent average speed of $\approx 1.4U$. When Re is low enough, for instance from figure 21, for approximatively $Re \leqslant 2500$, all vortices travel downstream faster than the developing turbulence, and a puff of stable length forms (Shimizu & Kida 2009). The turbulence can then be considered in statistical equilibrium. For much larger Re, for instance, $Re = 6000$ in our simulations, almost all vortices ejected from the vortex sheet are slower than the turbulence yet are intense enough to break down themselves. Precisely because they are slower, these new patches of turbulence are sown behind the passing interface, and end up aggregating to the existing turbulence, creating the impression of an overall smooth elongation. The slug can then be seen as a turbulent puff 'out of equilibrium'. However, the mechanisms through which the vortical activity is sustained within the slug itself are still unclear.

For intermediate values of Re, the propagation of the KH shed vortices has to be investigated statistically; some of them travel faster than the turbulent puff, while the slowest ones cause its spatial elongation. The turbulent puff is still out of equilibrium but its spatial elongation occurs now in jumps, as can be seen, for instance, in figure 13 at $Re = 3000$. More extensive data are needed to answer the question as to whether

https://doi.org/10.1017/S0022112010003435 Published online by Cambridge University Press

the transition from discontinuous to continuous elongation is abrupt or happens continuously when varying Re. A last regime of interest is defined by $\min C_{KH} \approx c_{LE}$. In this particular configuration, the puff is nearly in equilibrium but departs from the equilibrium turbulent puff every time a rare statistical event occurs, under the form of a slower KH shed vortex. The turbulent puff is expected to hesitate intermittently between keeping his puff-like shape or expanding spatially.

The range of Re for this intermediate regime can be determined, to a first approximation, by interpolation of $\min C_{KH} \approx c_{LE}$ from figure 21, which yields $Re \approx 2500$. A more conservative estimate of $Re \approx 2850$ is given by $\langle C_{KH} \rangle - \delta C_{KH} \approx c_{LE}$, i.e. when only rare statistical events travel slower than c_{LE}. This regime may well correspond to the spatiotemporally intermittent dynamics identified by Moxey & Barkley (2010) for Re between 2300 and 2600. A proper computational identification of this regime demands much larger domains, for instance $L = 150D$ in Moxey & Barkley (2010), as well as a more accurate way of getting statistics of C_{KH}. This regime bridges the gap in Re noticed by experimentalists between puffs and slugs (see, for instance, figure 2*b* in Wygnanski & Champagne 1973). The regime dependence on the relative sizes of $\min C_{KH}$ and c_{LE} can be summarized as follows:

(i) $\min C_{KH} > c_{LE}$: equilibrium puff;
(ii) $\min C_{KH} \approx c_{LE}$: intermittent regime;
(iii) $\min C_{KH} < c_{LE}$: slug expansion.

Finally, it would be interesting to investigate how this approach to spatio-temporal intermittency can be extended to other shear flows, such as the expansion of turbulent spots in a plane Couette flow or in the Blasius boundary layer.

Y.D. would like to thank D. S. Henningson for financial support during the years 2008–2009 and P. Manneville for fruitful discussions. A.P.W. was supported by a Marie-Curie Intra-European Fellowship grant.

Supplementary data are available at journals.cambridge.org/flm.

REFERENCES

Adrian, R. J. 2007 Hairpin vortex organization in wall turbulence. *Phys. Fluids* **19**, 041301.

Bandyopadhyay, P. R. 1986 Aspects of the equilibrium puff in transitional pipe flow. *J. Fluid Mech.* **163**, 439–458.

Binnie, A. M. & Fowler, J. S. 1947 A study of a double refraction method of the development of turbulence in a long cylindrical tube. *Proc. R. Soc. Lond.* A **192**, 32.

Darbyshire, A. G. & Mullin, T. 1995 Transition to turbulence in constant-mass-flux pipe flow. *J. Fluid Mech.* **289**, 83.

Duguet, Y., Pringle, C. & Kerswell, R. R. 2008*b* Relative periodic orbits in transitional pipe flow. *Phys. Fluids* **20**, 114102.

Duguet, Y., Schlatter, P. & Henningson, D. S. 2009 Localized edge states in plane Couette flow. *Phys. Fluids* **21**, 111–701.

Duguet, Y., Willis, A. P. & Kerswell, R. R. 2008*a* Transition in pipe flow: the saddle structure on the boundary of turbulence. *J. Fluid Mech.* **613**, 255–274.

Eckhardt, B., Schneider, T. M., Hof, B. & Westerweel, J. 2007 Turbulence transition in pipe flow. *Annu. Rev. Fluid Mech.* **39**, 447–468.

Faisst, H. & Eckhardt, B. 2003 Travelling waves in pipe flow. *Phys. Rev. Lett.* **91**, 224–502.

Gibson, J. F., Halcrow, J. & Cvitanovic, P. 2008 Visualizing the geometry of state space in plane Couette flow. *J. Fluid Mech.* **611**, 107–130.

Gibson, J. F., Halcrow, J. & Cvitanovic, P. 2009 Equilibrium and travelling wave solutions of plane Couette flow. *J. Fluid Mech.* **638**, 1–24.

https://doi.org/10.1017/S0022112010003435 Published online by Cambridge University Press

Hagen, G. H. L. 1839 Über die Bewegung des Wassers in engen zylindrischen Röhren. *Poggendorfs Annal. Physik Chemie* **16**, 423.

Halcrow, J., Gibson, J. F., Cvitanovic, P. & Viswanath, D. 2009 Heteroclinic connections in plane Couette flow. *J. Fluid Mech.* **621**, 365–376.

Herron, I. H. 1991 Observations on the role of vorticity on the stability of wall bounded flows. *Stud. Appl. Math.* **85**, 269–286.

Hof, B., DeLozar, A., Avila, M., Tu, X. & Schneider, T. M. 2010 Eliminating turbulence in spatially intermittent flows. *Science* **327**, 1491–1494.

Hof, B., van Doorne, C. W. H., Westerweel, J. & Nieuwstadt, F. T. M. 2005 Turbulence regeneration in pipe flow at moderate Reynolds numbers. *Phys. Rev. Lett.* **95**, 214–502.

Hof, B., van Doorne, C. W. H., Westerweel, J., Nieuwstadt, F. T. M., Faisst, H., Eckhardt, B., Wedin, H., Kerswell, R. R. & Waleffe, F. 2004 Experimental observation of nonlinear traveling waves in turbulent pipe flow. *Science* **305**, 1594–1597.

Itano, T. & Toh, S. 2001 The dynamics of bursting process in wall turbulence. *J. Phys. Soc. Japan* **70**, 703.

Joseph, D. D. & Carmi, S. 1969 Stability of Poiseuille flow in pipes, annuli, and channels. *Q. Appl. Math.* **26**, 575–599.

Kerswell, R. R. 2005 Recent progress in understanding the transition to turbulence in a pipe. *Nonlinearity* **18**, R17–R44.

Kerswell, R. R. & Tutty, O. R. 2007 Recurrence of travelling waves in transitional pipe flow. *J. Fluid Mech.* **584**, 69–102.

Leite, R. J. 1959 An experimental investigation of the stability of Poiseuille flow. *J. Fluid Mech.* **5**, 81.

Leonard, A. & Reynolds, W. C. 1985 Turbulence research by numerical simulation. In *Perspectives in Fluid Mechanics: Proceedings of a Symposium Held on the Occasion of the 70th Birthday of Hans Wolfgang Liepmann* (ed. D. Coles), Lecture Notes in Physics, vol. 320, p. 113. Springer.

Lindgren, E. R. 1958 The transition process and other phenomena in viscous flow. *Ark. Phys.* **12**, 1.

Lindgren, E. R. 1969 Propagation velocity of turbulent slugs and streaks in transition pipe flow. *Phys. Fluids* **12**, 418.

Mellibovsky, F. & Meseguer, A. 2009 Critical threshold in pipe flow transition. *Phil. Trans. R. Soc.* A **367**, 545–560.

Mellibovsky, F., Meseguer, A., Schneider, T. M. & Eckhardt, B. 2009 Transition in localized pipe flow turbulence. *Phys. Rev. Lett.* **103**, 054502.

Meseguer, A. & Trefethen, L. N. 2003 Linearized pipe flow to Reynolds number 10^7. *J. Comp. Phys.* **186**, 178–197.

Moxey, D. & Barkley, D. 2010 Distinct large-scale turbulent–laminar states in transitional pipe flow. *PNAS* **107**, 8091–8096.

Mullin, T. 2011 Transition to turbulence in a pipe: a historical perspective. *Annu. Rev. Fluid Mech.* **43**.

Nagata, M. 1990 Three-dimensional finite-amplitude solutions in plane Couette flow: bifurcation from infinity. *J. Fluid Mech.* **217**, 519–527.

Nishi, M., Unsal, B., Durst, F. & Biswas, G. 2008 Laminar-to-turbulent transition of pipe flows through puffs and slugs. *J. Fluid Mech.* **614**, 425–446.

Peixinho, J. & Mullin, T. 2006 Decay of turbulence in pipe flow. *Phys. Rev. Lett.* **96**, 094501.

Pfenniger, W. 1961 Transition in the inlet length of tubes at high Reynolds numbers. In *Boundary Layer and Flow Control* (ed. G. V. Lachman). NEW YORK: Pergamon.

Poiseuille, J. L. M. 1840 Recherches expérimentales sur le mouvement des liquides dans les tubes de très petits diamètres. *C. R. Acad. Sci.* **11**, 961.

Pringle, C. C. T., Duguet, Y. & Kerswell, R. R. 2009 Highly symmetric travelling waves in pipe flow. *Phil. Trans. R. Soc.* A **367**, 457–472.

Pringle, C. C. T. & Kerswell, R. R. 2007 Asymmetric, helical and mirror-symmetric travelling waves in pipe flow. *Phys. Rev. Lett.* **99**, 074502.

Priymak, V. G. & Miyazaki, T. 2004 Direct numerical simulation of equilibrium spatially localized structures in pipe flow. *Phys. Fluids* **16**, 4221–4234.

https://doi.org/10.1017/S0022112010003435 Published online by Cambridge University Press

Reuter, J. & Dempfer, D. 2004 Analysis of pipe flow transition. Part 1. Direct numerical simulation. *Theor. Comput. Fluid Dyn.* **17**, 273.

Reynolds, O. 1883 An experimental investigation of the circumstances which determine whether the motion of water shall be direct or sinuous and of the law of resistance in parallel channels. *Phil. Trans. R. Soc.* **174**, 935–982.

Schneider, T. M. & Eckhardt, B. 2009 Edge states intermediate between laminar and turbulent dynamics in pipe flow. *Phil. Trans. R. Soc.* A **367**, 577–587.

Schneider, T. M., Eckhardt, B. & Vollmer, J. A. 2007*a* Statistical analysis of coherent structures in transitional pipe flow. *Phys. Rev.* E **75**, 066313.

Schneider, T. M., Eckhardt, B. & Yorke, J. A. 2007*b* Turbulence transition and the edge of chaos in pipe flow. *Phys. Rev. Lett.* **99**, 034502.

Schneider, T. M., Gibson, J. F., Lagha, M., De Lillo, F. & Eckhardt, B. 2008 Laminar–turbulent boundary in plane Couette flow. *Phys. Rev.* E **78**, 037301.

Schneider, T. M., Marinc, D. & Eckhardt, B. 2010 Localized edge states nucleate turbulence in extended plane Couette cells. *J. Fluid Mech.* **646**, 441–451.

Shan, H., Ma, B., Zhang, Z. & Nieuwstadt, F. T. M. 1999 Direct numerical simulation of a puff and a slug in transitional cylindrical pipe flow. *J. Fluid Mech.* **387**, 39–60.

Shimizu, M. & Kida, S. 2008 Structure of a turbulent puff in pipe flow. *J. Phys. Soc. Japan* **77**, 114401.

Shimizu, M. & Kida, S. 2009 A driving mechanism of a turbulent puff in pipe flow. *Fluid Dyn. Res.* **41**, 045501.

Toh, S. & Itano, T. 1999 Low-dimensional dynamics embedded in a plane Poiseuille flow turbulence: traveling-wave solution is a saddle point? In *Proceedings of IUTAM Symposium on Geometry and Statistics of Turbulence* (ed. T. Kambe). Kluwer.

Viswanath, D. 2007 Recurrent motions within plane Couette turbulence. *J. Fluid Mech.*, **580**, 339–358.

Viswanath, D. 2009 The critical layer in pipe flow at high Reynolds number. *Phil. Trans. R. Soc.* **367**, 561–576.

Waleffe, F. 1997 On the self-sustaining process in shear flows. *Phys. Fluids* **9**, 883–900.

Waleffe, F. 1998 Three-dimensional coherent states in plane shear flows. *Phys. Rev. Lett.* **81**, 4140–4143.

Wang, J., Gibson, J. & Waleffe, F. 2007 Lower branch coherent states in shear flows: transition and control. *Phys. Rev. Lett.* **98**, 204501.

Wedin, H. & Kerswell, R. R. 2004 Exact coherent structures in pipe flow: travelling wave solutions. *J. Fluid Mech.* **508**, 333–371.

Willis, A. P. & Kerswell, R. R. 2007 Critical behavior in the relaminarization of localized turbulence in pipe flow. *Phys. Rev. Lett.* **98**, 14501.

Willis, A. P. & Kerswell, R. R. 2008 Coherent structures in local and global pipe turbulence. *Phys. Rev. Lett.* **100**, 124–501.

Willis, A. P. & Kerswell, R. R. 2009 Turbulent dynamics of pipe flow captured in a reduced model: puff relaminarization and localized 'edge' states. *J. Fluid Mech.* **619**, 213–233.

Willis, A. P., Peixinho, J., Kerswell, R. R. & Mullin, T. 2009 Experimental and theoretical progress in pipe flow transition. *Phil. Trans. R. Soc.* A **366**, 2671–2684.

Wygnanski, I. J. & Champagne, F. H. 1973 On transition in a pipe. Part 1. The origin of puffs and slugs and the flow in a turbulent slug. *J. Fluid Mech.* **59**, 281–351.

https://doi.org/10.1017/S0022112010003435 Published online by Cambridge University Press